Cell-Penetrating Peptide TAT-HuR-HNS3 Suppresses Proinflammatory Gene Expression via Competitively Blocking Interaction of HuR with Its Partners

Ke Wang,*,†,1 Haibin Tong,‡,1 Yitian Gao,‡ Lan Xia,*,† Xin Jin,*,† Xiaoxue Li,*,† Xianlu Zeng,*,† Istvan Boldogh,§ Yueshuang Ke,*,† and Xueqing Ba*,†

Proinflammatory cytokines/chemokines are commonly regulated by RNA-binding proteins at posttranscriptional levels. Human Ag R (HuR)/embryonic lethal abnormal vision-like 1 (ELAVL1) is one of the well-characterized RNA-binding proteins that increases the stability of short-lived mRNAs, which encode proinflammatory mediators. HuR employs its nucleocytoplasmic shuttling sequence (HNS) domain, interacting with poly(ADP-ribose) polymerase 1 (PARP1), which accounts for the enhanced poly-ADP-ribosylation and cytoplasmic shuttling of HuR. Also by using its HNS domain, HuR undergoes dimerization/oligomerization, underlying the increased binding of HuR with proinflammatory cytokine/chemokine mRNAs and the disassociation of the miRNA-induced silencing complex from the targets. Therefore, competitively blocking the interactions of HuR with its partners may suppress proinflammatory mediator production. In this study, peptides derived from the sequence of the HuR-HNS domain were synthesized, and their effects on interfering HuR interacting with PARP1 and HuR itself were analyzed. Moreover, cell-penetrating TAT-HuR-HNS3 was delivered into human and mouse cells or administered into mouse lungs with or without exposure of TNF-α or LPS. mRNA levels of proinflammatory mediators as well as neutrophil infiltration were evaluated. We showed that TAT-HuR-HNS3 interrupts HuR–PARP1 interaction and therefore results in a lowered poly-ADP-ribosylation level and decreased cytoplasmic distribution of HuR. TAT-HuR-HNS3 also blocks HuR dimerization and promotes Argonaute 2–based miRNA-induced silencing complex binding to the targets. Moreover, TAT-HuR-HNS3 lowers mRNA stability of proinflammatory mediators in TNF-α–treated epithelial cells and macrophages, and it decreases TNF-α–induced inflammatory responses in lungs of experimental animals. Thus, TAT-HuR-HNS3 is a promising lead peptide for the development of inhibitors to treat inflammation-related diseases. ***The Journal of Immunology*****, 2022, 208: 2376–2389.**

The RNA-binding proteins (RBPs) regulate RNA metabolism, such as alternative splicing, mRNA stability, polyadenylation, subcellular localization, and translation. Functional dysregulation of RBPs has been associated with a variety of human diseases (1, 2). Human Ag R (HuR)/embryonic lethal abnormal vision-like protein 1 (ELAVL1), one of the best studied RBPs, stabilizes short-lived mRNAs by associating with AU-rich elements (AREs) or a U-rich sequence in 3′-untranslated regions (3′-UTRs) (3–6). HuR has been shown to stabilize a large number of target mRNAs, many of which encode proteins implicated in inflammation and cancer.

Predominantly, HuR plays a critical role in modulating proinflammatory mediators' expression in response to stress, infections, and other pathophysiological processes (7–13). For instance, HuR targets the 3′-UTR of inflammatory mediator *IL-6* mRNA and enhances its stabilization in periodontitis (14). IL-13 induces airway inflammation in allergic diseases. HuR associates with the 3′-UTR of *IL-13* mRNA, promoting mRNA stability and translation (15). In a mouse model, HuR also modulates proinflammatory cytokines/chemokines (*Cxcl2*, *Tnf*, and *Il-1β*) production by associating with mRNA 3′-UTRs, augmenting LPS-induced acute pulmonary inflammation (16).

Additionally, HuR is highly abundant in many tumor cells and regulates expression of genes correlating with tumor aggressiveness (17). A well-known example is the stabilization of cyclooxygenase-2 (COX-2) by HuR in colorectal cancer. HuR binds to the 3′-UTR of *COX-2* mRNA to antagonize miR-16 function that promotes rapid *COX-2* mRNA decay (18). BCL-2 plays a critical role in cancer cell survival, and HuR regulates *BCL-2* mRNA stability and translation via associating with the mRNA 3′-UTR in HL60

*Key Laboratory of Molecular Epigenetics of Ministry of Education, Northeast Normal University, Changchun, Jilin, China; †School of Life Science, Northeast Normal University, Changchun, Jilin, China; ‡Zhejiang Provincial Key Laboratory for Water Environment and Marine Biological Resources Protection, College of Life and Environmental Science, Wenzhou University, Wenzhou, China; and §Department of Microbiology and Immunology, University of Texas Medical Branch at Galveston, Galveston, TX

[1]K.W. and H.T. contributed equally to this work.

ORCIDs: 0000-0002-2655-4197 (X.Z.), 0000-0003-1518-4271 (Y.K.).

Received for publication January 4, 2022. Accepted for publication March 17, 2022.

This work was supported by National Natural Science Foundation of China Grants 32170591 and 31970686 (to X.B.) and 32170724 and 31801182 (to Y.K.), Natural Science Foundation of Jilin Province Grant 20190201183JC (to X.L.), and by National Institute of Allergic and Infectious Diseases Grant AI062885 (to I.B.).

Address correspondence and reprint requests to Dr. Xueqing Ba or Dr. Yueshuang Ke, Key Laboratory of Molecular Epigenetics of Ministry of Education, School of Life Sciences, Northeast Normal University, 5268 Renmin Street, Changchun, Jilin 130024, China (X.B) or School of Life Science, Northeast Normal University, Changchun, Jilin 130024, China (Y.K.). E-mail addresses: baxq755@nenu.edu.cn (X.B.) or keys585@nenu.edu.cn (Y.K.)

The online version of this article contains supplemental material.

Abbreviations used in this article: Act D, actinomycin D; Ago2, Argonaute 2; ARE, AU-rich element; COX-2, cyclooxygenase-2; CPP, cell-penetrating peptide; HNS, HuR nucleocytoplasmic shuttling sequence; HuR, human Ag R; i.n., intranasal(ly); IP, interfering peptide; miRISC, miRNA-induced silencing complex; MLE, murine lung epithelial; PARP1, poly(ADP-ribose) polymerase 1; PARylation, poly-ADP-ribosylation; RBP, RNA-binding protein; RRM, RNA recognition motif; 3′-UTR, 3′-untranslated region; WB, Western blotting.

leukemia cells and A431 carcinoma cells (19). HuR also binds to the *VEGF* mRNA 3′-UTR to modulate tumor growth and angiogenesis (20–23). Deviation in mRNA stability results in significant changes in the quantities of mature mRNAs and proteins (24–29). Thus, HuR has emerged as an attractive drug target for inflammation and cancer therapies.

HuR is composed of three highly conserved canonical RNA recognition motif (RRM) domains. RRM1 and RRM2 domains are responsible for its interaction with target mRNAs, and RRM3 is needed for HuR associating with poly(A) tail. HuR is primarily located in the nucleus. The HuR nucleocytoplasmic shuttling sequence (HNS) domain, located between RRM2 and RRM3, is responsible for HuR nucleocytoplasmic shuttling and determines the localization of HuR (30). RRM3 and the C-terminal of HNS are indispensable for HuR oligomerization (31, 32). HuR increases the half-life of mRNAs coding proinflammatory mediators by forming oligomer, and it promotes the disassociation of miRNA-induced silencing complexes (miRISCs) from mRNA (33–35), thus attenuating the cleavage activity of miRISC (32, 36–39).

Posttranslational modifications that determine HuR's abundance and intracellular localization constitute the major aspects for its functional regulations (12, 40, 41). Studies have addressed the effects of phosphorylation, methylation, ubiquitination, and neddylation on HuR function, underpinning the alteration of HuR's protein stability, affinity for RNA binding, and subcellular localization (40, 42–45). Recent studies showed that, in response to inflammatory stimuli, poly ADP-ribosylation (PARylation) of HuR, mainly catalyzed by poly(ADP-ribose) polymerase 1 (PARP1), upregulates the stability of inflammatory mediators' mRNA by promoting the cytoplasmic distribution of HuR and its oligomerization along target RNAs (16, 32). Thus, blocking the induced HuR-PARP1 interaction or HuR's oligomerization holds the promise to treat inflammatory diseases.

HuR employs its HNS domain to achieve the interaction with PARP1, and D226 in the HNS domain is the major site for HuR PARylation (16). Additionally, the HNS domain, especially its C-terminal one third, also mediates HuR's oligomerization, which is enhanced by HuR PARylation (32). In this study, peptides derived from the sequence of the HuR-HNS domain were synthesized, and the effects on interfering interactions of HuR with PARP1 and HuR itself were analyzed. Moreover, cell-penetrating TAT-HuR-HNS3 was delivered into mouse cells or administrated into mouse lungs with or without exposure of TNF-α or LPS. TAT-HuR-HNS3 interrupts HuR–PARP1 interaction, resulting in a lowered PARylation level and decreased nucleocytoplasmic shuttling of HuR. Moreover, TAT-HuR-HNS3 blocks HuR dimerization and elevates Argonaute 2 (Ago2)–associated miRISC binding to the targets. Importantly, this cell-penetrating peptide (CPP) lowers proinflammatory mediators' mRNA production in epithelial cells and macrophages, and mitigates neutrophil infiltration in mouse lungs induced by TNF-α exposure.

Materials and Methods

Reagents and Abs

Transcription inhibitor actinomycin D (Act D, A1410), PARP1 inhibitor PJ34 (P4365), and LPS (L2630) were from Sigma-Aldrich (St. Louis, MO). PARP1 inhibitor olaparib (AZD2281) was from Selleck Chemicals (Houston, TX). Recombinant human TNF-α (300-01A) was from PeproTech (Cranbury, NJ). CPPs were provided by Dangang Biotechnology (Hangzhou, China) and proven free of endotoxin by the using the ToxinSensor single test kit (L00856-20, GenScript, Jiangsu, China). Lipofectamine 2000 (Invitrogen) was used for transfection of plasmids. HuR Ab (3A2, sc-5261) and mAb against PARP1 (B-10, sc-74470) were purchased from Santa Cruz Biotechnology (Santa Cruz, CA). β-Tubulin Ab (HC101), mouse anti-GAPDH Ab (HC301-01), β-actin Ab (HC201-01), GFP Ab (HT801), and His Ab (HT501) were purchased from TRANS (Beijing, China). mAb against poly(-ADP-ribose) (PAR) (ALX-804-220) was purchased from Alexis (San Diego, CA). FLAG Ab (F1804) was from Sigma-Aldrich (St. Louis, MO). Ab against lamin A/C (10298-1-AP) was from ProteinTech (Wuhan, China).

Cell culture

Human kidney epithelial cells (HEK293) and mouse macrophages (RAW-264.7) were grown in DMEM supplemented with 10% (v/v) FBS (HyClone), 10 mM glutamine, 100 IU/ml penicillin, and 100 μg/ml streptomycin. Immortalized type 2 murine lung epithelial (MLE) cells (MLE-12) were grown in DMEM supplemented with 2% (v/v) FBS, 10 mM glutamine, 100 IU/ml penicillin, and 100 μg/ml streptomycin. Cells were regularly tested for mycoplasma contamination.

Constructs

GST and GST-HuR plasmids were provided by Dr. Myriam Gorospe (Laboratory of Cellular and Molecular Biology, National Institute on Aging, National Institutes of Health). His-HuR was constructed by subcloning HuR amplicons into His-tag vector (PET30a) with EcoRI and XhoI restriction endonuclease sites. To construct FLAG-Ago2 plasmid, Ago2 was amplified by PCR using cDNA from HEK293 cells as the template and then cloned into the vector pCMV-N-FLAG with HindIII and EcoRI restriction endonuclease sites. To construct GFP-murine HuR plasmid, murine HuR was amplified by PCR using cDNA from MLE-12 cells as the template and then cloned into the vector pAcGFP-C1 with BgIII and EcoRI restriction endonuclease sites. GFP-TAT, GFP-HuR-HNS3, and GFP-TAT-HuR plasmids were constructed by subcloning TAT, HuR-HNS, and TAT-HuR into the vector pAcGFP-C1 with BglII and EcoRI restriction endonuclease sites.

Expression and purification of recombinant proteins

Recombinant proteins were generated as we described previously. Briefly, recombinant proteins were expressed in *Escherichia coli* strain BL21. Log-phase cells were treated with 0.5 mM IPTG and 50 μM $ZnSO_4$ for 3 h at 37°C. Cell pellets (collected at 4000 × *g* for 10 min) were lysed in buffer containing 20 mM HEPES (pH 7.5), 120 mM NaCl, 5% glycerol, and a protease inhibitor mixture (11836153001, Roche, Mannheim, Germany). Cell lysates were centrifuged at 18,000 × *g* for 25 min at 4°C to obtain the supernatant. The supernatant (with 0.5% Nonidet P-40) was collected and incubated with balanced and reduced glutathione 4B (17075601, GE Healthcare Life Sciences, Uppsala, Sweden) or Ni-NAT agarose beads (30210, Qiagen, Hilden, Germany) on a rotator at 4°C for 3 h or overnight. Beads were washed and eluted, and the purified recombinant proteins were confirmed by Western blotting (WB).

Protein pull-down assay

The whole-cell lysate from MLE-12 or purified recombinant His-HuR was incubated with GST and GST-HuR immobilized on glutathione Sepharose 4B beads in the presence or absence of peptides (10 μM HuR-HNS1, HuR-HNS2, and HuR-HNS3) at 4°C for 3 h or overnight. Beads were washed four times with TEN100, then 2× loading buffer equal to the volume of the beads was added and heated at 95°C for 5 min. SDS-PAGE was performed to detect HuR-PARP1 and HuR-HuR interactions.

Fluorescence microscopy

MLE-12 or RAW264.7 cells were plated on collagen precoated cover glasses (Roche Applied Sciences) and stimulated by TNF-α (10 ng/ml) or mock treated for 3 h. Cells were fixed with acetone/methanol (1:1) for 20 min at room temperature, or dried and stored when needed. Then, cells were rinsed and permeabilized using 0.1% (w/v) Triton X-100 diluted in PBS (PBST) for 5 min. Cells were incubated with 1% BSA for 1 h at room temperature. HuR Ab (1:100) was then added in PBST, followed by incubation for 1 h at 37°C. After washing the cells with PBST, secondary Ab (Alexa Fluor 594 goat anti-mouse IgG) was applied. After washing, cells were mounted with DAPI (H-1200-10, Vector Laboratories, Burlingame, CA). Six to 10 randomly selected fields were imaged using a ×60 objective on a confocal microscope (Nikon, Tokyo, Japan). Quantification of cytoplasmic HuR was conducted by using ImageJ software (v1.41, National Institutes of Health). The total HuR amount was measured first, and then the cytoplasmic HuR amount was obtained by subtracting the nuclear HuR amount from that of the total. The redistribution of HuR was estimated by dividing the cytoplasmic amount of HuR by that of total. The value of the mock-treated group was taken as 1 and other groups were normalized to the mock-treated group.

In vitro PARylation assay

A PARylation assay was performed with a slight modification of a method described previously (16), using the HT universal chemiluminescent PARP assay

kit (Trevigen, Gaithersburg, MD). Briefly, GST and GST-HuR immobilized on glutathione Sepharose 4B beads were incubated with recombinant PARP enzyme and PARP mixture at room temperature for 1 h. After three washes with Nonidet P-40 lysis buffer, the bound proteins were analyzed by WB.

Cell death detection

Detection of apoptotic cells was performed using an annexin V–FITC apoptosis analysis kit (AO2001-10, Sungene Biotech, Tianjin, China), following the manufacturer's instructions. Briefly, cells were harvested and washed with cold PBS, and then annexin V–FITC was added to cell suspension for 10 min at room temperature. After washing twice with PBS, cells were incubated in propidium iodide solution for 5 min. Flow cytometry was performed by using FACSCanto II (BD Biosciences), and data were analyzed with FACSDiva software (BD Biosciences).

Cell viability assay

MLE-12 cells were seeded in 96-well plates at a concentration of 5×10^4 cells per well in 100 μl of culture medium in the absence or presence of various amounts of peptides (10, 25, 50 μM). Cells were maintained for 24 h at 37°C and MTT (M2128, Sigma-Aldrich, St. Louis, MO) assays were performed. Briefly, after incubation, 10 μl of the MTT reagent was added (at a final concentration of 0.5 g/l) to each well, followed by incubation at 37°C for 4 h. Solubilization solution (100 μl) was added into each well for overnight in the incubator. The absorbance of the formazan product was measured at 570-nm wavelength using an ELx800 absorbance microplate reader (BioTek Instruments, Winooski, VT).

Reverse transcription and quantitative real-time PCR

Cells were lysed and total RNAs were isolated using TRIzol (15596-026, Invitrogen, Carlsbad. CA). RNA concentrations were determined spectrophotometrically ($OD_{260}/OD_{280} > 1.9$), and RNA was stored at −80°C. Mouse lungs (100 mg) were fully homogenized in 1 ml of TRIzol (15596-026, Invitrogen, Carlsbad, CA) and centrifuged at 13,000 × *g* at 4°C for 5 min and RNAs were extracted. The reverse transcription of total RNA into cDNA was conducted by using a Takara reverse transcription kit (RR037A, Takara, Beijing, China). Quantitative real-time PCR was performed to detect *Cxcl2*, *Tnf*, and *Il-1β* mRNAs (16), using cellular *β-actin* as an internal control (sequences of primers are listed in Table I). The level of mRNA was expressed as a fold change using the ΔΔCt method.

Stability of mRNA

To measure the stability of the inflammatory mediator's mRNA, a classical approach was applied (16, 46). Cells were exposed to TNF-α (10 ng/ml) for 1 h for an immune boost, then the transcription inhibitor Act D (10 μg/ml) was added to the medium with or without the maintenance of TNF-α (with or without10 μM olaparib or TAT-HuR-HNS3) for 0, 1, 2, 3, and 4 h. RNAs were isolated using TRIzol (15596-026, Invitrogen, Carlsbad, CA), and quantitative real-time PCR was performed using an Applied Biosystems thermocycler. The relative abundance of *Tnf*, *Cxcl2*, and *Il-1β* mRNAs was determined by normalizing to *β-actin* using the ΔΔCt method (sequences of primers are listed in Table I). The relative amount of mRNA without Act D treatment was taken as 100%.

Coimmunoprecipitation and WB analysis

Parallel cultures of cells (1×10^7 MLE-12, RAW264.7, or HEK293 cells transfected with GFP, GFP-TAT, GFP-HuR-HNS3, GFP-TAT-HuR-HNS3, and GFP-HuR plasmids) were TNF-α– (10 ng/ml) or mock-treated for 3 h and then lysed using lysis buffer (9803, Cell Signaling Technology, Danvers, MA) (50 mM Tris-HCl [pH 7.5], 150 mM NaCl, 1 mM EDTA, 1 mM EGTA, 1% Nonidet P-40) containing 2.5 mM sodium pyrophosphate, 1 mM glycerophosphate, and protease inhibitors. Cell lysates were clarified (14,000 × *g* at 4°C for 30 min) and then incubated with protein A/G beads (HY-K0202, MCE, Shanghai, China) coupled with anti-HuR Ab or anti-GFP Ab for 3 h at 4°C with rotation. Beads were washed three times with lysis buffer and the proteins were eluted by boiling in 1× loading buffer. Eluted proteins were separated by SDS-PAGE electrophoresis and WB was performed to detect the immunoprecipitated PARP1, PARylation, or HuR using mouse anti-PARP1, mouse anti-poly(ADP-ribose), or mouse anti-HuR Abs. The signals were detected by using ECL Plus chemiluminescent detection reagents (S6010, US Everbright, Hong Kong, China). β-Tubulin and GAPDH were used as controls.

Table I. Sequences of PCR primers and EMSA RNA oligonucleotides

Gene Name	Sequence
β-Actin	5′-AACAGTCCGCCTAGAAGCAC-3′ (forward)
	5′-CGATGACATCCGTAAAGACC-3′ (reverse)
Cxcl2	5′-TCAATGCCTGAAGACCC-3′ (forward)
	5′-TGGTTCTTCCGTTGAGG-3′ (reverse)
Il-1β	5′-CAGGATGAGGACATGAGCACC-3′ (forward)
	5′-CTCTGCAGACTCAAACTCCAC-3′ (reverse)
Tnf	5′-TACTGAACTTCGGGGTGATTGGTCC-3′ (forward)
	5′-CAGCCTTGTCCCTTGAAGAGAACC-3′ (reverse)
β-ACTIN	5′-CTCCATCCTGGCCTCGCTGT-3′ (forward)
	5′-GCTGTCACCTTCACCGTTCC-3′ (reverse)
TNF	5′-TGCACTTTGGAGTGATCGG-3′ (forward)
	5′-TCAGCTTGAGGGTTTGCTAC-3′ (reverse)
AU-rich RNA oligonucleotide	5′-AUUUAUUUAUUUAUUUAUUUAUUUA-3′
Cxcl2 RNA oligonucleotide	5′-CUAUGUAUUUAUUUAUUUAUUAAUU-3′

RNA EMSA

Interactions of HuR or its mutants with target RNAs were analyzed by RNA EMSA. Briefly, proteins (with or without PARylation) were dissolved in the EMSA interaction buffer (3 mM $MgCl_2$, 40 mM KCl, 5% glycerol, 2 mM DTT, 2 μg of tRNA) and incubated with 2 nM 5′-biotin–labeled RNA oligonucleotides (sequences of oligonucleotides are listed in Table I) for 10 min at room temperature. The reaction mixtures were applied to 6% polyacrylamide gels in low-ionic-strength buffer (0.5× TBE [Tris-borate-EDTA]) and electrophoresed for 2 h at 4°C. Visualization of HuR-RNA complexes was carried out with a LightShift chemiluminescent RNA EMSA kit (20158, Thermo Fisher Scientific, Waltham, MA) with modification.

RNA Immunoprecipitation

To isolate RNP complexes, a whole-cell lysate from peptide-treated MLE-12 cells or FLAG-Ago2–overexpressing HEK293 cells was precleared and then immunoprecipitated by using protein A/G agarose coated with anti-HuR or anti-FLAG Ab (2 μg). After the beads were washed with NT2 buffer (50 mM Tris-HCl [pH 7.5], 150 mM NaCl, 1 mM $MgCl_2$, and 0.05% Nonidet P-40), the mRNA was isolated by using an RNA sample total RNA kit (DP419, Tiangen, Beijing, China). The RNA levels in beads-Ab-protein/mRNA complex for each sample were assessed by reverse transcription–coupled quantitative real-time PCR (sequences of primers are listed in Table I).

Animals and challenge

Ten-week-old female and male BALB/c mice (20–25 g) were purchased from Changsheng Bio-technology (Benxi, Liaoning, China). Mice were housed in a specific pathogen–free facility at Northeast Normal University (Changchun, Jilin, China) and allowed unlimited access to sterilized feed and water. They were maintained at 23 ± 1°C and kept under a 12-h light/12-h dark cycle. All experiments were conducted in accordance with the Chinese Council on Animal Care Guidelines. Randomly selected groups of mice (50% male, 50% female) were challenged with TNF-α (20 ng per lung) in 60 μl of pH-balanced saline solution (pH 7.4) under mild anesthesia via the intranasal (i.n.) route. TAT-HuR-HNS3 (100 ng per lung) in a 60-μl solvent (5% DMSO in saline) was administered i.n. 1 h before TNF-α challenge.

Evaluation of airway inflammation

Responses of airways to TNF-α challenge were examined as we described previously (47). After euthanasia, tracheae were cannulated and lungs were lavaged by two instillations of 0.6 ml of ice-cold PBS. Bronchoalveolar lavage fluids (BALFs) were centrifuged (800 × *g* for 5 min at 4°C), and the resulting supernatants were stored at −80°C for further analysis. Total cell counts in the BALF were determined from an aliquot of the cell suspension by using a hemocytometer. Cytospin preparations were made by using a Shandon Cytospin 4 cytocentrifuge (Thermo Fisher Scientific, Waltham, MA). Cells were stained with modified Wright–Giemsa using a HEMA-TEK 2000 slide stainer (Thermo Fisher Scientific, Waltham, MA) for differential cell counts. Lungs were removed and fixed in 10% buffered formalin, followed by paraffin embedding. Five-micrometer cross-sections were stained with H&E to identify neutrophils as described previously (47). Randomly, 10 fields of each sample were photographed by using an Olympus BX53P microscope system.

Statistical analysis

All experiments were performed independently at least three times for each determination. The data are expressed as the mean ± SEM. Results were analyzed for significant differences using one-way or two-way ANOVA. Differences were considered significant at $p < 0.05$ ($*p < 0.05$, $**p < 0.01$, $***p < 0.001$).

Results

Selection of HuR-HNS peptides for blocking the interactions of HuR-PARP1 and HuR-HuR

To select potential peptide blocking the interactions of HuR-PARP1 and HuR-HuR, three peptides with sequences derived from the HuR-HNS domain and with 6 aa overlapped were designed and synthesized, named as HuR-HNS1, HuR-HNS2, and HuR-HNS3 (Fig. 1A). Recombinant GST or GST-HuR was purified and incubated with cell lysate generated from MLE-12 cells in presence or absence of individual peptide (10 μM). Results of pull-down assays showed that HuR-HNS3, but not HuR-HNS1 and HuR-HNS2, blunted the interaction of HuR–PARP1 (Fig. 1B), and the impact was concentration-dependent (Fig. 1C). To further address whether HuR-HNS3 has an effect on HuR PARylation, an in vitro PARylation assay was performed as described in *Materials and Methods*. Bead-coated GST or GST-HuR was incubated with or without PARP1 in the absence or presence of HuR-HNS3. Incubation with PARP1 resulted in strong PARylation of GST-HuR but not GST, which was markedly decreased due to the addition of HuR-HNS3 or PARP1 inhibitor PJ34 (48) (Fig. 1D).

A previous study revealed that PARylation enhances HuR oligomerization (32), and, interestingly, the last one-third (C-terminal) of HuR-HNS was proven to mediate HuR's self-interaction (31, 32). Thus, we proposed that the peptide HuR-HNS3 may also impair HuR dimerization. To this end, bead-coated GST and GST-HuR were incubated with recombinant His-HuR in the presence or absence of individual peptides. Results showed that indeed HuR-HNS3, but not other peptides, greatly inhibited HuR–HuR interaction (Fig. 1E) and that the effect was concentration-dependent (Fig. 1F).

TAT-HuR-HNS3 shows efficient cell penetration without eliciting cytotoxicity

In light of the well-characterized advantage of naturally derived TAT peptide in cell delivery (49–51), we assessed the efficacy of cellular uptake of TAT-tagged HuR-HNS3 (TAT-HuR-HNS3). To visualize and quantify, TAMRA was covalently conjugated to the N-terminal of TAT. Epithelial cells that line the inner surface of the respiratory tract and the gastrointestinal tract are often the first place attacked by a pathogen or allergen, and thus they are ideally suited to support studies in many fields, including cancer, inflammation, and gene regulation; thus, MLE-12 cells were incubated with TAMRA-TAT-HuR-HNS3 (10 μM) for various times and intracellular TAMRA signals were detected by flow cytometry. Result showed that TAT-HuR-HNS3 was delivered into the cells from 15 min on. The fluorescence-positive cell rate was ~70% at 60 min and reached a maximum (~80%) at 90 min (Fig. 2A). In parallel, the intracellular distribution of TAMRA-TAT-HuR-HNS3 was examined by confocal microscopy. Results showed that the signals were located in both cytoplasmic and nuclear compartments of MLE-12 cells after 90 min of exposure of TAMRA-TAT-HuR-HNS3 (Fig. 2B). The efficiency of cellular uptake was also confirmed by addition of this peptide to murine RAW264.7 macrophages, as this type of cells represents the major group of the immune system and are involved in inflammation occurrence and resolution. Microscopic imaging showed punctate florescence, which implied an endocytosis pathway (Supplemental Fig. 1A, 1B). Moreover, artificially synthesized polyarginine (R9) peptide with the distinct ability to cross cell plasma membranes (52) also exhibited high delivery efficiency when R9-tagged HuR-HNS3 was added to MLE-12 cells (Supplemental Fig. 1C, 1D). To test whether TAT-HuR-HNS3 has toxic effects, MTT and annexin V/propidium iodide staining coupled flow cytometry assays (Fig. 2C, 2D, Supplemental Fig. 1E) were performed. Results showed that TAT and TAT-HuR-HNS3 have no detectable effect on the metabolic activity of cells (Fig. 2C) or cell viability (Fig. 2D, Supplemental Fig. 1E), even at a high concentration (50 μM).

TAT-HuR-HNS3 inhibits HuR PARylation and suppresses HuR nucleocytoplasmic translocation

Cytoplasmic translocation under stress is a necessary step for HuR functioning in the stabilization of target mRNAs (16, 53). PARylation of HuR affects its subcellular translocation (16); thus, we first investigated the effects of TAT-HuR-HNS3 on HuR–PARP1 interaction and PARylation of HuR. Preliminary study showed that maximum cytoplasmic translocation of HuR and PARylation of whole-lysate proteins in cells occur at 3 h (Supplemental Fig. 2A, 2B). Thus, MLE-12 or RAW264.7 cells were administrated with DMSO, TAT, or TAT-HuR-HNS3 for 1 h and stimulated with TNF-α for another 3 h, and then a protein immunoprecipitation assay was conducted by using HuR Ab. WB results showed that TAT-HuR-HNS3 but not TAT blocked the interaction of HuR–PARP1 and the PARylation of HuR (Fig. 3A, 3B, Supplemental Fig. 2C, 2D). To exclude the possibility that HuR-HNS3 peptide itself was PARylated and might serve as a competitive inhibitor of the enzyme in general, GFP, GFP-TAT, GFP-HuR-HNS3, or GFP-TAT-HuR-HNS3 were overexpressed in HEK293 cells, and immunoprecipitation was performed by using GFP Ab. None of these proteins was PARylated upon TNF-α challenge (Fig. 3C), indicating that although HuR-HNS3 mediates HuR–PARP1 interaction and contains the amino acid being PARylated, the occurrence of PARylation of D226 in HNS needs an appropriate conformation of full-length HuR or the HuR-HNS3 domain to accommodate PARP1 to catalyze PARylation on D226. Next, we further addressed whether TAT-HuR-HNS3 plays a key role as a PARP1 inhibitor in general. Olaparib, a U.S. Food and Drug Administration–approved PARP1 inhibitor (54), or TAT-HuR-HNS3 was used, and the results revealed that TAT-HuR-HNS3 has no effect on the PARylation of whole-lysate proteins (Fig. 3D). Thereafter, the effect of TAT-HuR-HNS3 on HuR cytoplasmic translocation was assessed. Immunofluorescence labeling analysis of the subcellular distribution of HuR revealed that the TNF-α challenge–induced increase in cytoplasmic abundance of HuR was suppressed by administration of TAT-HuR-HNS3 but not TAT, and the effect was similar to that of olaparib (Fig. 3E, Supplemental Fig. 2E). Lower cytoplasmic HuR levels caused by TAT-HuR-HNS3 administration were further verified by WB (Fig. 3F, Supplemental Fig. 2F). TNF-α exposure and peptide treatment have no effect on HuR expression (Supplemental Fig. 2G, 2H). These data indicated that TAT-HuR-HNS3 treatment blocks the interaction of HuR and PARP1, leading to impaired PARylation of HuR, and thereby the mitigated cytoplasmic translocation of HuR.

TAT-HuR-HNS3 inhibits HuR dimerization and increases the association of miRISC with target RNAs

To explore the effect of TAT-HuR-HNS3 on HuR's mRNA-stabilizing function in cytoplasm, we first investigated whether the peptide blocks the association of HuR with target mRNAs. MLE-12 cells were pretreated with peptides (TAT, TAT-HuR-HNS3) or PARP1 inhibitor and then stimulated with TNF-α for 3 h. Cell lysate was immunoprecipitated with HuR Ab, and an RNA immunoprecipitation assay was conducted. The results showed that the *Tnf* mRNA bound to HuR was increased significantly after TNF-α challenge, and this increase was suppressed by pretreatment of TAT-HuR-HNS3, but not TAT (Fig. 4A). It has been reported that self-interaction of HuR is beneficial for its substrate association (55). Thus, we explored the effect of TAT-HuR-HNS3 on HuR dimerization. GFP- or GFP-HuR–overexpressing HEK293 cells were incubated with TAT-HuR-HNS3 for 1 h, followed by TNF-α stimulation. Three hours later, the cell extracts were subjected to protein

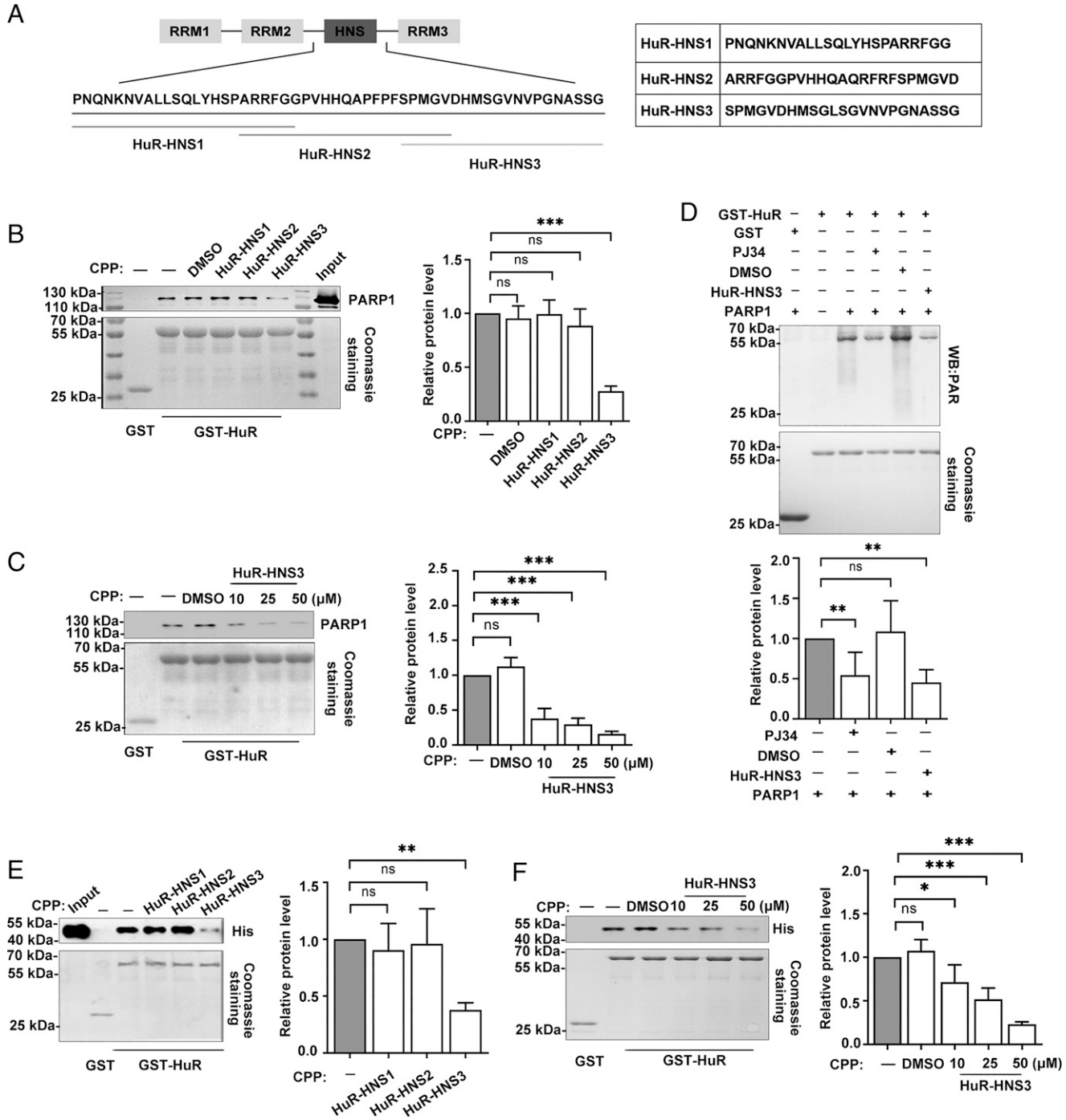

FIGURE 1. HuR-HNS3 blocks interactions of HuR with its partners. (**A**) Amino acid sequences of the HuR-HNS domain and individual peptides. (**B** and **C**) HuR-HNS3 inhibits HuR–PARP1 interaction in a concentration-dependent manner. GST and GST-HuR were incubated with equal amounts of whole-cell extracts from MLE-12 cells in the presence of peptides or not. Levels of pulled-down PARP1 were detected by WB. Shown is a representative of three independent experiments (left panels), and PARP1 levels were quantified by analysis of band density using ImageJ software (v1.41, National Institutes of Health). The value of the band density for GST-HuR alone was taken as 1 (right panels, $n = 3$). (**D**) HuR-HNS3 depresses PARylation level of HuR. Equal amounts of bead-coated GST and GST-HuR were incubated with or without PARP1 in the presence of peptide or not, and then subjected to WB to detect PARylation levels. Shown is a representative of three independent experiments (upper panel), and the HuR PARylation level was quantified by using ImageJ software (v1.41, National Institutes of Health), and the value of the band density for GST-HuR incubated with PARP1 was taken as 1 (lower panel, $n = 3$). (**E** and **F**) HuR-HNS3 inhibits HuR–HuR interaction in a concentration-dependent manner. GST and GST-HuR were incubated with equal amounts of His-tagged HuR as well as peptides. Levels of pulled-down His-HuR were detected by WB. Shown is the representative of three independent experiments (left panels), and His-HuR levels were quantified by analysis of band density using ImageJ software (v1.41, National Institutes of Health) and are shown in the right panels. The value of the band density for GST-HuR alone was taken as 1 (right panels, $n = 3$). Data are expressed as mean ± SEM. A one-way ANOVA was applied to determine the significance of the difference. $^{*}p < 0.05$, $^{**}p < 0.01$, $^{***}p < 0.001$; ns, not significant.

immunoprecipitation by using GFP Ab. In response to TNF-α exposure, the amount of endogenous HuR in the protein complex precipitated by GFP Ab from GFP-HuR–expressing cells was increased, and this increase was significantly diminished by prior TAT-HuR-HNS3 administration. In controls, endogenous HuR was not precipitated by GFP Ab from GFP-expressing cells (Fig. 4B).

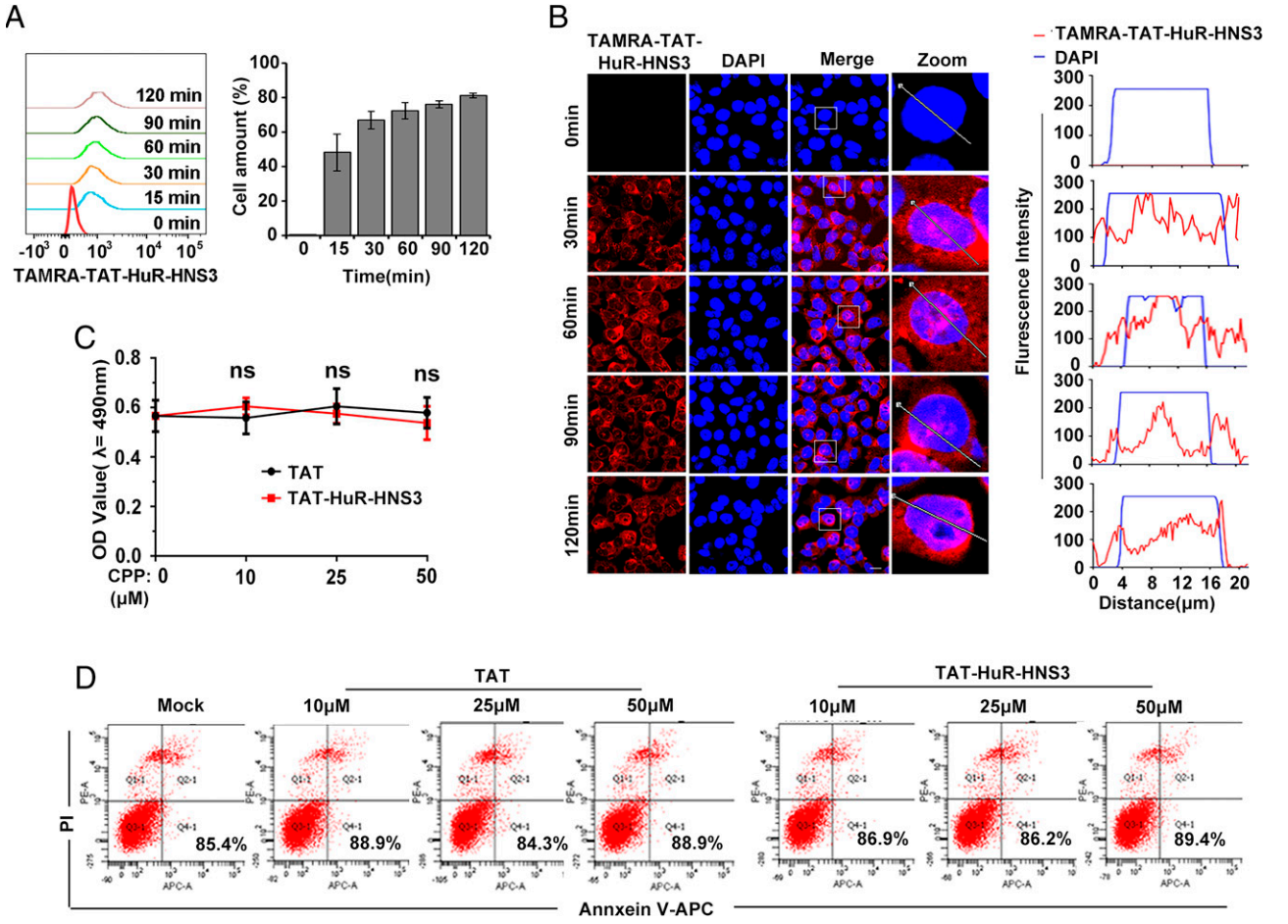

FIGURE 2. Cell-penetrating peptide delivers HuR-HNS3 into the cells without eliciting cytotoxicity. (**A**) TAT-HuR-HNS3 displays high cell-penetrating capability. MLE-12 cells were incubated with fluorescent peptides (10 μM) for various times and examined by flow cytometry. Representative fluorescence intensities were analyzed using FlowJo software (left panel), and positive cell rates from three independent experiments were quantified at the indicated time points (right panel). (**B**) Cellular distribution of TAT-HuR-HNS3. MLE-12 cells were mock treated or incubated with fluorescent peptides at 37°C for various times as indicated, then fixed and observed under a ×60 objective on a confocal microscope. Representative images from three independent experiments are shown in the left panel. Scale bar, 20 μm. The profiles in the right panel show the fluorescence intensity of TAMRA-TAT-HuR-HNS3 from line scans in the magnified views of the boxed areas from the merged images in the left panel, which were analyzed by Image Pro Plus software (red, TAMRA-TAT-HuR-HNS3; blue, DAPI). (**C** and **D**) Biological compatibility of TAT-HuR-HNS3. MLE-12 cells were incubated with various concentrations (10, 25, and 50 μM) of TAT-HuR-HNS3 for 24 h at 37°C. An MTT assay was performed to assess cell metabolic activity, and results show the average OD value of three independent experiments. Annexin V/propidium iodide (PI) staining–coupled flow cytometry was performed to detect cell death, and representative data of three independent experiments are shown (D). Data are presented as the mean ± SEM in (C). A one-way ANOVA was applied to determine the significance of the difference. ns, not significant, compared with TAT treatment.

To further address the effects of peptides on the oligomerization of HuR along the target RNAs, recombinant GST-HuR was subjected to PARylation or not, and then RNA EMSA was performed by using 2 nM ARE-containing RNA probes (25 nt, sequences shown in Table I) in the presence or absence of HuR-HNS3. Peptides HuR-HNS1 and HuR-HNS2 were used as controls. PARP1 activity enhanced the binding of both monomeric and oligomeric HuR with the tandem ARE-containing probes (Fig. 4C) as well as *Cxcl2* 3′-UTR–derived probes (Supplemental Fig. 3A), and the enhancement was markedly decreased by the addition of inhibitor olaparib (10 μM) or peptide HuR-HNS3 (10 μM), but it was scarcely impaired by peptides HuR-HNS1 and HuR-HNS2 (Fig. 4C, Supplemental Fig. 3A). The inhibitory effect of peptide HuR-HNS3 was dose-dependent (Fig. 4D, Supplemental Fig. 3B).

3′-UTRs of mammalian mRNAs can be as long as 10 kb or more and are associated with miRISC and HuR (37). Considering that oligomerization of HuR promotes miRISC dissociation and that Ago2 is critical for compartmentalization of miRISC (56–59), we speculated that occupancy of HuR oligomer on the 3′-UTR could be perturbed by HuR-HNS3, and the perturbation in turn stabilizes Ago2 on the target mRNAs. To test this idea, HEK293 cells were transfected with FLAG-Ago2 plasmid and stimulated with TNF-α (10 ng/ml) for 3 h. TAT-HuR-HNS1, TAT-HuR-HNS2, TAT-HuR-HNS3, or PARP1 inhibitor was applied 1 h prior to TNF-α exposure. RNA immunoprecipitation was performed using FLAG Ab. Immunoprecipitated RNAs were converted into cDNA by using oligo(dT) primers to assess the level of *TNF* mRNA by using quantitative real-time PCR (primer sequences are listed in Table I). Results showed that PARP1 inhibitor increased the level of *TNF* mRNA bound to Ago2, and the effect was also achieved by prior administration of TAT-HuR-HNS3, but not that of TAT-HuR-HNS1 and TAT-HuR-HNS2 (Fig. 4E).

TAT-HuR-HNS3 decreases the stability of proinflammatory mediators' mRNA

Because TAT-HuR-HNS3 interferes with HuR PARylation, HuR self-interaction, as well as its competition with miRISC, the potential anti-inflammatory activity of this peptide was determined. First,

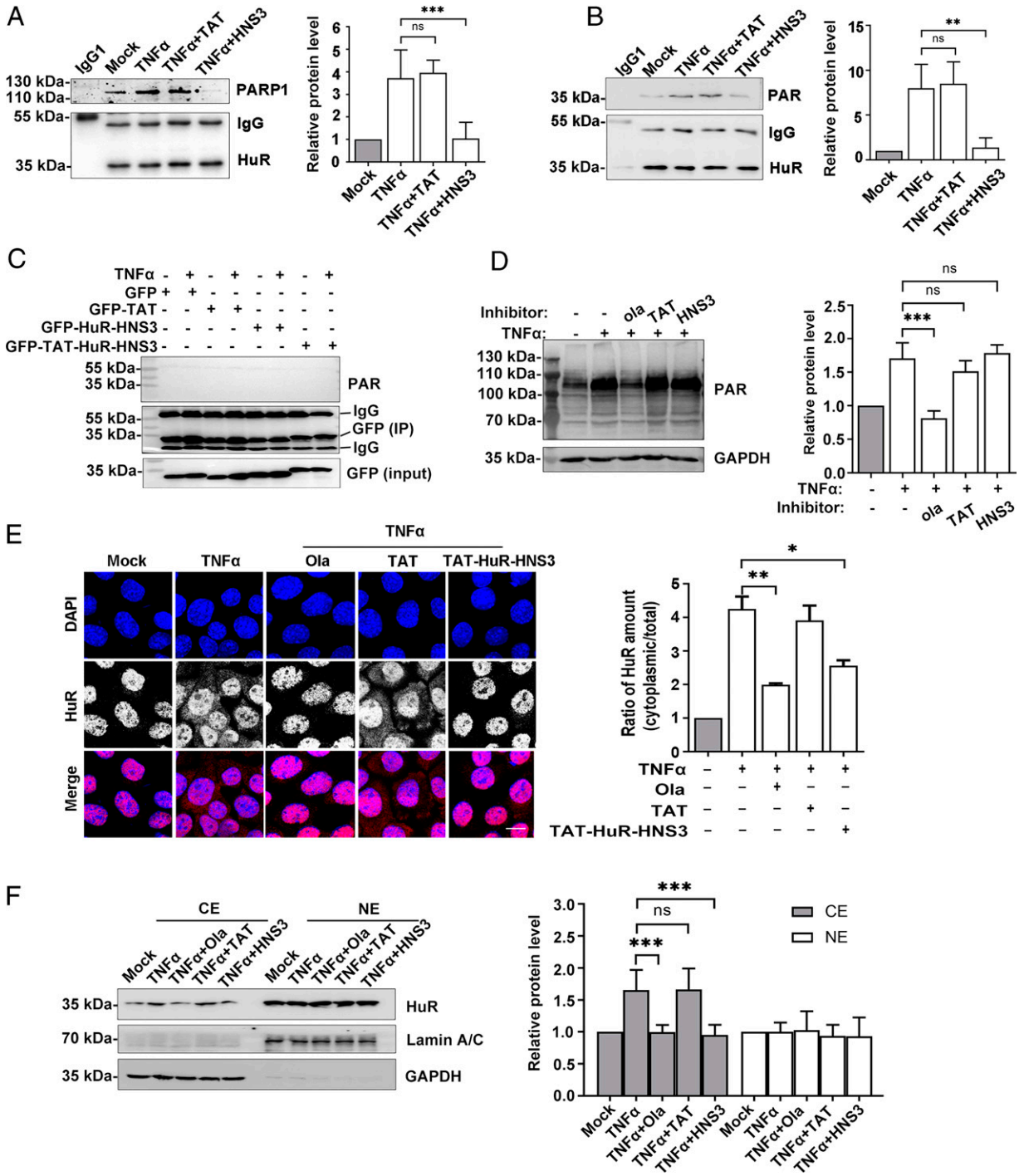

FIGURE 3. TAT-HuR-HNS3 inhibits HuR PARylation and suppresses HuR nucleocytoplasmic translocation. (**A** and **B**) TAT-HuR-HNS3 blocks TNF-α–induced HuR–PARP1 interaction and abrogates the increase in HuR's PARylation. MLE-12 cells were administered TAT or TAT-HuR-HNS3 (10 μM) for 1 h, followed by stimulation with TNF-α (10 ng/ml) for another 3 h, and protein precipitation was carried out by using HuR Ab; WB was performed to analyze HuR–PARP1 interaction using PARP1 Ab or the HuR PARylation level of HuR using an Ab against PAR polymer. Shown are results representative of three independent experiments (left panels). Levels of immunoprecipitated PARP1 or PARylation or HuR were quantified by analysis of band density using ImageJ software (v1.41, National Institutes of Health), and the value of the band density for the mock-treated group was taken as 1 (right panels, $n = 3$). (**C**) There is no PARylation occurring on TAT-HuR-HNS3 itself. HEK293 cells transfected with GFP, GFP-TAT, GFP-HuR-HNS3, or GFP-TAT-HuR-HNS3 were mock treated or TNF-α treated (10 ng/ml). Protein immunoprecipitation was carried out by using GFP Ab; WB was performed to analyze PARylation of these peptides, and representative results of three independent experiments are shown. (**D**) TAT-HuR-HNS3 has no role as a PARP1 inhibitor. MLE-12 cells pretreated with olaparib (Ola) or peptides were challenged with TNF-α (10 ng/ml). The level of protein PARylation of whole lysates was analyzed by WB. Representative results of three independent experiments are shown (left panel); PARylation levels were quantified by using ImageJ software (v1.41, National Institutes of Health). The value of the band density for the mock-treated group was taken as 1 (right panel, $n = 3$). (**E** and **F**) TAT-HuR-HNS3 inhibits TNF-α–induced cytoplasmic translocation of HuR. With or without a 1-h preadministration of Ola (10 μM), TAT, or TAT-HuR-HNS3 (10 μM), MLE-12 cells were stimulated with TNF-α (10 ng/ml) or not for 3 h at 37°C. (E) Then, the cells were washed and immunofluorescence staining was performed by using HuR Ab. HuR distribution was observed with a ×60 objective on a confocal microscope. Randomly, 6–10 fields (~60 cells) in each group were selected for quantification as shown in the right panel. Representative images from three independent experiments are shown in the left panel, and *(Figure legend continues)*

mRNA levels of proinflammatory genes were examined. Due to the role of pulmonary alveoli epithelial cells in the onset of inflammation, mRNAs of *Tnf*, *Cxcl2*, and *Il-1β* in MLE-12 cells were examined, and results showed a significant increase in the expression levels of these genes in response to TNF-α stimulation, and the increase was significantly lowered by the pre-addition of TAT-HuR-HNS3 but not TAT. A similar inhibitory effect of the PARP1 inhibitor olaparib was observed (Fig. 5A). The effects of TAT-HuR-HNS3 on TNF-α– or LPS-induced mRNA production of proinflammatory mediators were similar when RAW264.7 cells were used (Supplemental Fig. 4).

Next, the stability of mRNAs of *Tnf*, *Cxcl2*, and *Il-1β* with or without TAT-HuR-HNS3 administration was determined. MLE-12 cells were exposed to TNF-α for 1 h, followed by addition of the transcription inhibitor Act D with or without the maintenance of TNF-α (with or without TAT-HuR-HNS3). The levels of the remaining mRNAs were determined by using quantitative real-time PCR. The *Tnf*, *Cxcl2*, and *Il-1β* mRNA levels in mock-treated cells rapidly declined after Act D addition. TNF-α stimulation sustained the mRNA stability (much more than 4 h), which was significantly suppressed by TAT-HuR-HNS3 administration (~3.5 h) (Fig. 5B).

TAT-HuR-HNS3 attenuates TNF-α–induced lung inflammation

Given the proven effect of TAT-HuR-HNS3 on expression of proinflammatory cytokines/chemokines in cell cultures, we further examined the potential roles of the peptide in vivo. The mice were pretreated with saline or TAT-HuR-HNS3 (100 ng per lung, i.n.) for 1 h, followed by i.n. challenge of TNF-α (20 ng per lung). Levels of *Tnf* and *Cxcl2* mRNA increased to 60- and 20-fold, respectively, in response to stimulation for 12 h, and the increase was significantly diminished by prophylactic application of TAT-HuR-HNS3, whereas TAT-HuR-HNS3 alone did not significantly induce inflammatory gene expression (Fig. 6A). In parallel, BALF analysis was carried out. Twelve-hour TNF-α challenge elicited a robust increase in the number of neutrophils, reaching $>4\times 10^5$ cells/ml, which was significantly lowered to $<1.5\times 10^5$ by the prophylactic administration of TAT-HuR-HNS3 (Fig. 6B, 6C). Moreover, the subepithelial accumulation of leukocytes in lung tissues was also assessed. TNF-α markedly induced neutrophil accumulation, which was attenuated by preadministration of TAT-HuR-HNS3 (Fig. 6D). Few inflammatory cells were present in the subepithelial area of mice challenged with saline or TAT-HuR-HNS3 alone. Taken together, these data indicate that TAT-HuR-HNS3 is potent to attenuate stimuli-induced lung inflammation.

Discussion

Regulation of proinflammatory cytokine/chemokine expression usually is achieved at both the transcriptional and posttranscriptional levels. Modulation of mRNA stability provides rapid and flexible control, and it is particularly important in coordinating the initiation and resolution of inflammation (41). HuR, one of the best studied RBPs determining cytoplasmic mRNA fate, has emerged as an important regulator of mRNA stability of proinflammatory factors that is implicated in different pathologies, particularly inflammation and cancer (7, 9). In the current study, a HuR-HNS domain sequence was derived and the CPP TAT-HuR-HNS3 was proven potent to inhibit proinflammatory cytokine/chemokine expression and attenuate lung inflammation (Fig. 6).

To date, there are plenty of HuR-targeting inhibitors, which are well characterized to interrupt the disease process (60). The ongoing HuR-targeted therapeutic strategies include silencing HuR expression, inhibiting HuR's translocation from the nucleus to the cytoplasm, and blocking the association of HuR with target RNAs (44, 60–62). For instance, MS-444, a chrysanthone-like small-molecule compound, has an anticancer effect in malignant glioma cells. It has an effect on attenuating microglial migration and invasion via inhibiting HuR translocation to the cytoplasm (63). A cumarin-derived small-molecule inhibitor, CMLD-2, competitively binds to HuR and disrupts HuR–ARE interaction, exhibiting an antitumor effect. It decreases HuR mRNA and the mRNAs of HuR-regulated proteins (Bcl2 and p27) in lung cancer cells (64). However, HuR plays fundamental roles in a variety of RNA metabolism processes, including splicing, polyadenylation, exporting, stabilization, as well as translation efficiency, either constitutively or in response to inductive stimulation (36, 65). This situation may hamper the aspiration of the strategies such as silencing of HuR or blocking the substrate binding or cytoplasmic translocation of HuR in clinical applications. HuR is normally located in the nucleus, and the increased subcellular localization in cytoplasm is regarded as a marker of diseases (60, 66). HuR's cellular distribution is largely dependent on post-translational modifications within the HNS region. Previous studies documented that an inflammatory stimulus induced the interaction of PARP1 with HuR, which results in PARylation of the latter at D226, and this modification is indispensable for HuR cytoplasmic translocation (16). Once in the cytosolic compartment, HuR stabilizes mRNAs by forming oligomer to promote the disassociation of miRISC from the binding site in the 3′-UTRs to attenuate its cleavage ability (32, 36, 37). HuR's PARylation is also beneficial for its self-interaction and the enhanced disassociation of miRISC from the binding sites, and thereby the stabilization of proinflammatory gene mRNAs (32). Thus, blocking the inflammatory stimuli–induced PARP1–HuR and/or HuR–HuR interactions can be considered a viable strategy to treat inflammation-related diseases.

Interfering peptides (IPs) have been recognized as valuable substances to specifically target protein–protein interactions and receiving increasing attention (67). The protein–protein interactions are often associated with various diseases; thus, designing and utilizing IPs in oncology and molecular therapeutics represent an emerging pharmacological strategy in precision medicine (68). For example, the BIG3-PHB2 (the brefeldin A–inhibited guanine nucleotide-exchange protein 3–prohibitin 2) complex plays a crucial role in E2/ERα signaling modulation in breast cancer cells. A specific inhibition of the BIG3–PHB2 interaction using the ERα activity regulator synthetic peptide derived from the α-helical BIG3 sequence resulted in a significant antitumor effect (69). Estrogen feedback actions may underlie many other physiological processes; thus, other than the specificity of the IPs, the pathological implications of the targeted protein–protein interactions should be a great concern in

the percentage of cytoplasmic HuR was quantified using Image J (v1.41, National Institutes of Health) as described in *Materials and Methods*. The value of the intensity for the mock-treated group was taken as 1 (right panel, $n = 3$). Scale bar, 20 μm. (F) Cytoplasm and nucleus fractions were isolated and the HuR amount was assessed by WB, taking the amount of GAPDH and lamin A/C as loading controls, respectively. Shown are the representative results of three independent experiments (left panel), and the levels of HuR expression were quantified by analysis of band density using ImageJ software (v1.41, National Institutes of Health), and the value of the band density for the mock-treated group was taken as 1 (right panel, $n = 3$). The data are presented as the mean ± SEM. A one-way ANOVA was applied to determine the significance of the difference. $^*p < 0.05$, $^{**}p < 0.01$, $^{***}p < 0.001$ (ns, not significant), compared with the sample incubated with TNF-α alone. CE, cytosolic extract; NE, nuclear extract.

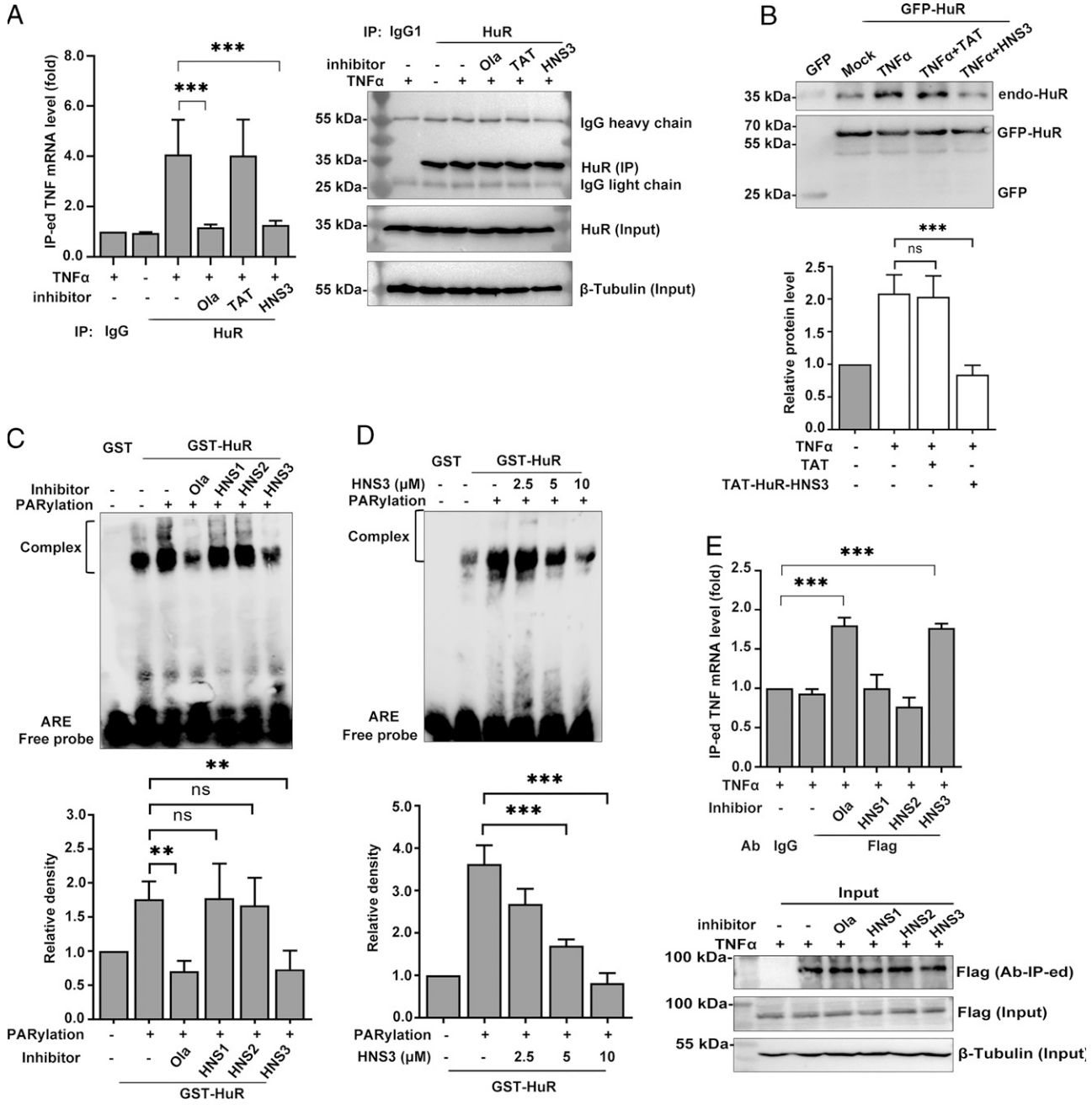

FIGURE 4. TAT-HuR-HNS3 inhibits HuR oligomerization along target RNAs and promotes miRISC-RNA association. (**A**) TAT-HuR-HNS3 suppresses HuR association with target RNA. MLE-12 cells pretreated with the the PARP1 inhibitor olaparib (Ola) or peptides (TAT, TAT-HuR-HNS3) were challenged with TNF-α (10 ng/ml), and 3 h later whole lysate was immunoprecipitated with HuR Ab. Real-time PCR was performed to detect the immunoprecipitated *TNF* mRNA level. The IgG immunoprecipitated mRNA amount in each experiment was taken as 1. Data from three independent experiments are presented as mean ± SEM (left panel). Right panel shows input and immunoprecipitated HuR protein levels as controls. (**B**) TAT-HuR-HNS3 interrupts TNF-α–induced HuR–HuR interaction. MLE-12 cells transfected with GFP or GFP-HuR were pretreated with 10 μM TAT and TAT-HuR-HNS3 (labeled as HNS3) for 1 h, and then stimulated with TNF-α (10 ng/ml) for another 3 h. GFP Ab was used for immunoprecipitation, and WB was performed to detect the interaction of GFP-HuR with endo-HuR using HuR Ab. Shown are representative results of three independent experiments (upper panel), and level of immunoprecipitated endo-HuR was quantified by analysis of band density using ImageJ software (v1.41, National Institutes of Health), and the value of the band density for the mock-treated group was taken as 1 (lower panel, $n = 3$). The data are presented as the mean ± SEM. (**C** and **D**) Binding of HuR with the ARE motif–containing RNA oligonucleotide is blocked by HuR-HNS3. GST or GST-HuR was incubated with PARP1 in the presence of Ola or HuR-HNS1, HuR-HNS2, and HuR-HNS3 (labeled as HNS1, HNS2, and HNS3), and then 2 nM ARE motif–containing RNA probe was added and EMSA was performed. Shown are representative results of three independent experiments (upper panels), and binding of HuR was quantified by analysis of band density using ImageJ software (v1.41, National Institutes of Health); the value of the band density for the GST-HuR alone group was taken as 1 (lower panels, $n = 3$). The data are presented as the mean ± SEM. (**E**) TAT-HuR-HNS3 promotes Ago2 association with target RNA. HEK293 cells transfected with FLAG-Ago2 were pretreated with or without 10 μM of Ola, TAT-HuR-HNS1, TAT-HuR-HNS2, or TAT-HuR-HNS3 as described above and then stimulated with TNF-α for 3 h. RNA immunoprecipitation was conducted using IgG or FLAG Ab. The bead-Ab-protein/mRNA complexes were subjected to PCR to detect the pulled-down *TNF* mRNA level. The IgG immunoprecipitated mRNA amount in each experiment was taken as 1. Data from three independent experiments are presented as mean ± SEM (upper panel). The lower panel shows input and immunoprecipitated FLAG-Ago2 protein levels as controls. A one-way ANOVA was applied to determine the significance of the difference. $^{**}p < 0.01$, $^{***}p < 0.001$; ns, not significant. IP, immunoprecipitation.

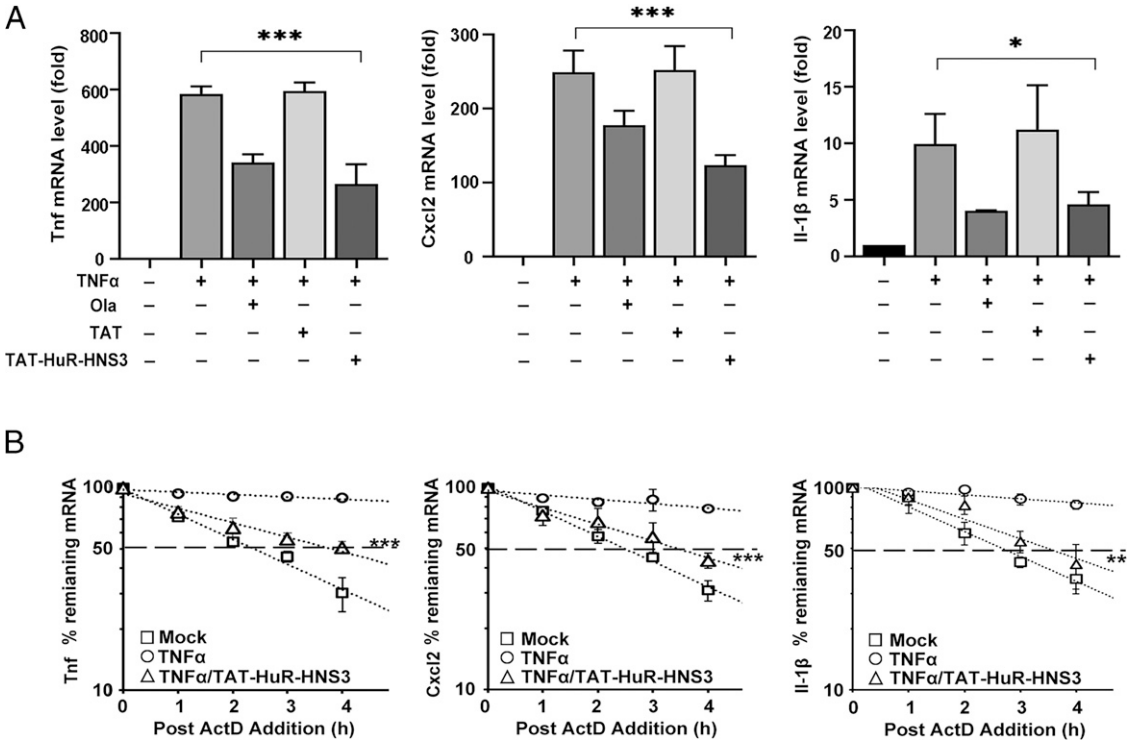

FIGURE 5. TAT-HuR-HNS3 downregulates mRNA stability of inflammatory mediators. (**A**) TAT-HuR-HNS3 decreased TNF-α–induced expression of proinflammatory mediators *Tnf*, *Cxcl2*, and *Il-1β*. MLE-12 cells were pretreated with olaparib (Ola), TAT, or TAT-HuR-HNS3 (10 μM) for 1 h, and then stimulated with TNF-α (10 ng/ml) for 3 h. RNA extraction was conducted and real-time PCR was performed to assess the indicated mRNA levels. Data were normalized to *β-Actin* mRNA, and relative gene expression of mock-treated cells in each experiment was taken as 1. Data from three independent experiments are presented as mean ± SEM. (**B**) TAT-HuR-HNS3 decreased proinflammatory mediators' mRNA half-lives in TNF-α–exposed cells. MLE-12 cells were exposed to TNF-α (10 ng/ml) for 1 h to boost the transcription of proinflammatory mediators and then subjected to transcriptional inhibition with or without TNF-α maintenance (with or without 10 μM TAT-HuR-HNS3) for various times as indicated. Real-time PCR was performed to assess the remaining mRNA levels of *Tnf*, *Cxcl2*, and *Il-1β*. Data were normalized to *β-actin* mRNA, and the relative remaining mRNA levels of mock-treated cells in each experiment were taken as 1. Data from three independent experiments are presented as mean ± SEM. A one- or two-way ANOVA was applied to determine the significance of the difference. $*p < 0.05$, $**p < 0.01$, $***p < 0.001$, compared with the sample with TNF-α challenge alone.

the selection of IPs. Previous studies have revealed that HuR's HNS domain mediates the interactions of PARP1–HuR as well as HuR–HuR in response to inflammatory stimulations (16, 32). To determine whether the IPs are capable of interfering with these interactions, we shortened HNS domain into three overlapped peptides to screen the functional inhibitory segment. HuR-HNS3, derived from the C-terminal (the last one third) of the HuR-HNS domain, was able to block PARP1–HuR interaction and HuR's PARylation both in vitro and in vivo (Figs. 1B–D, 3A, 3B, Supplemental Fig. 2C, 2D), and to mitigate HuR's cytoplasmic redistribution (Fig. 3E, 3F, Supplemental Fig. 2E, 2F). In contrast, this peptide also blocks HuR's self-interaction and the binding of HuR oligomer along with RNA in vivo and in vitro (Figs. 1E, 1F, 4A–D, Supplemental Fig. 3A, 3B), which in turn accounts for the crippled competition with miRISC for target association (Fig. 4E), and thereby for the impaired stabilization of proinflammatory genes' mRNA (Fig. 5). Therefore, the IP TAT-HuR-HNS3 could be satisfying for it can competitively inhibit the pathogenic protein interactions under inflammatory conditions.

The transport of mRNAs from the nucleus to the cytoplasm involves adapter proteins that bind the mRNA as well as receptor proteins that interact with the nuclear pore complex. HuR, serving as an mRNA adaptor, exhibits heat shock–sensitive interactions with transportin 2 (Trn2), or with ligands such as pp32 and APRIL, which contain leucine-rich nuclear export signals recognized by the export receptor CRM1 (70). The interaction of HuR with these partners also involves its HNS region. Whether the segment of the C-terminal of HNS is crucial for the interacting interface between HuR and other proteins engaged in nuclear export and whether the inhibitory peptide HuR-HNS3 can competitively block these interactions remain to be further investigated.

CPPs are a class of peptides possessing a significant capacity for membrane transduction and could be exploited to deliver various biologically active cargoes into the cells, including small molecules, plasmid DNA, small interfering RNA, therapeutic proteins, and nanoparticles (71). TAT was the first discovered CPP 30 y ago (50, 72). Afterwards, hundreds of additional CPPs have been discovered, and similar to TAT, many of the CPPs were derived from natural proteins or peptides, including viral proteins, heparin-binding proteins, DNA/RBPs, homeoproteins, signal peptides, and antimicrobial peptides (71, 73, 74). In the group of synthetic CPPs, polyarginine of 8–10 mer is the most widely studied because of its high efficiency in cellular uptake (75). In the current study, both TAT and R9 were conjugated to the N-terminal of HuR-HNS3, and data showed that TAT-HuR-HNS3 or R9-HuR-HNS3 penetrated the cell membrane with high efficacy and was distributed in both the nucleus and cytoplasm (Fig. 2A, 2B, Supplemental Fig. 1A–D), revealing that these CPPs are efficient drug delivery vehicles for therapeutic administration of HuR-HNS3 peptide.

How CPPs internalize into cells has long been a topic of debate: some CPPs seemingly enter cells through an endocytic mechanism and others directly penetrate the cell membrane (73), depending on the properties of CPPs or transported cargoes (e.g., concentration, structure), cell types (e.g., membrane lipid composition), and the

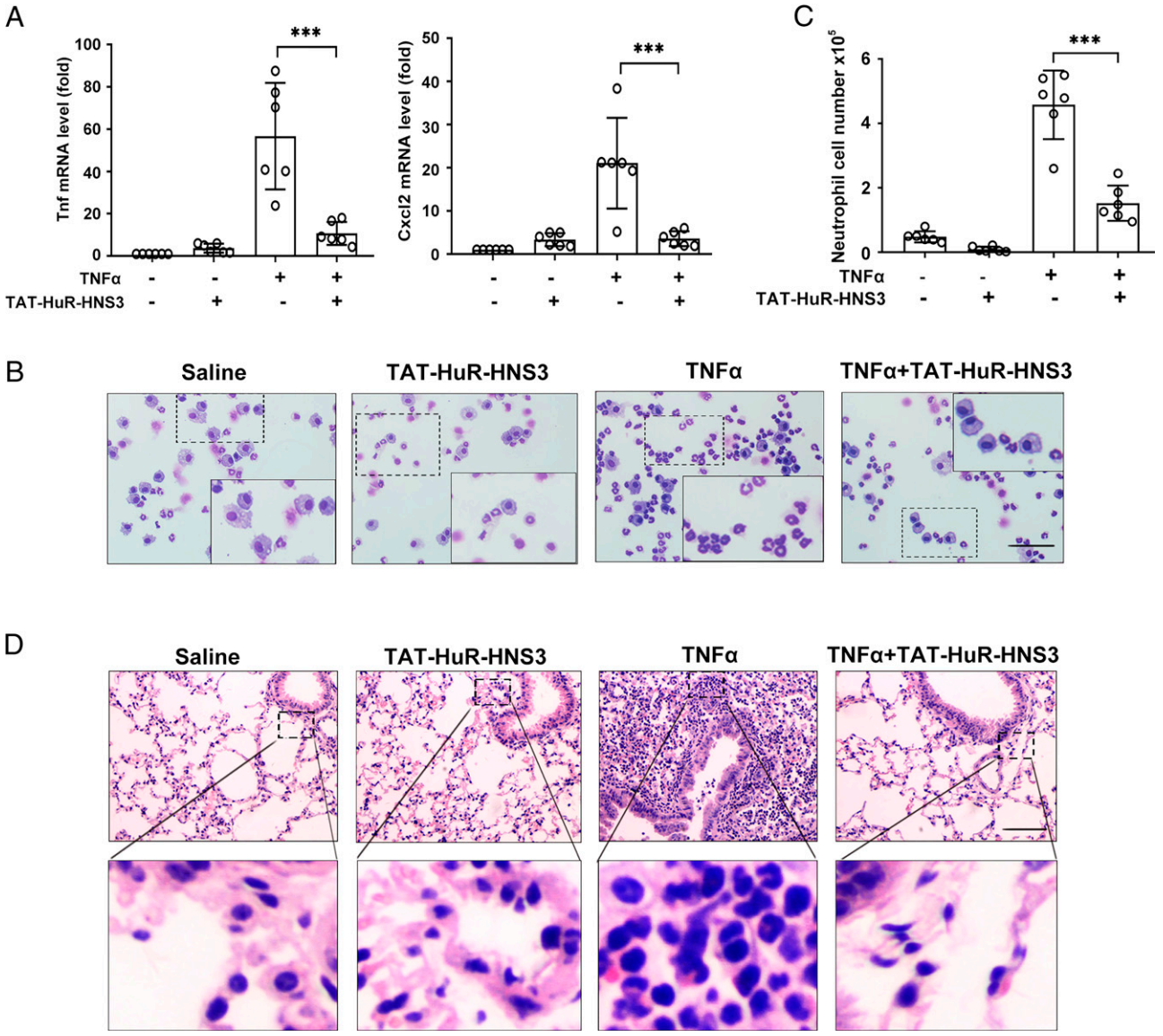

FIGURE 6. TAT-HuR-HNS3 attenuates TNF-α–induced lung inflammation. (**A**) TAT-HuR-HNS3 inhibits proinflammatory gene expression in the lungs of mice. Mice were pretreated (i.n.) with saline or TAT-HuR-HNS3 (100 ng per lung) for 1 h and then stimulated (i.n.) with TNF-α (20 ng per lung) for another 12 h. Lung tissues were collected, after which mRNA levels were examined by real-time PCR. Data were normalized to *β-actin* mRNA, and relative gene expression of saline-treated cells in each experiment was taken as 1. Six mice per group were analyzed in two independent experiments, and the data are presented as the mean ± SEM. (**B**) Visual depiction of leukocytes in BALF derived from mouse lungs. Mice were treated as described above. Twelve hours later, mice were euthanized and lavaged. Cells from BALF were fixed and stained with modified Wright–Giemsa stain. Scale bar, 100 μm. Ten randomly selected fields of view per cytospin slide were imaged. Results are representative of two independent experiments with a total of six mice in each group. (**C**) TAT-HuR-HNS3 interrupts neutrophil influx in the lungs of mice induced by TNF-α (i.n.). The number of neutrophils in BALF was determined after modified Wright–Giemsa staining on coated slides by two independent investigators in a blinded manner. The average neutrophil number of saline-treated cells in each experiment was taken as 1. Six mice per group were analyzed in two independent experiments, and the data are presented as the mean ± SEM. (**D**) Mice were treated as described above. Lung tissue sections were processed for staining with H&E to examine the subepithelial accumulation of leukocytes. Scale bar, 100 μm. Ten randomly selected fields of view per cytospin slide were imaged. Results are representative of two independent experiments with a total of six mice in each group. A one-way ANOVA indicated the significance between the TNF-α/TAT-HuR-HNS3 and TNF-α groups. ***$p < 0.001$. BALF, bronchoalveolar lavage fluid.

experimental conditions (such as pH and temperature) (71). So far, four different pathways, including micropinocytosis (76), caveolin-mediated endocytosis, clathrin-mediated endocytosis, and clathrin- and caveolin-independent endocytosis have been used to describe endocytosis (71). When RAW264.7 cells were incubated with TAMRA-TAT-HuR-HNS3, fluorescence signals were exhibited as round particles in the cytoplasm; however, this was not observed in MLE-12 cells, which implied that there are two deferent pathways of TAT-HuR-HNS3 entering into RAW264.7 and MLE-12 cells. In a therapeutic setting, further investigations are needed to increase the half-life of the peptide by a tailored delivery system to the target pathological tissue, thereby protecting the peptide from enzymatic degradation (77).

Taken together, the current study proved a substantial anti-inflammation effect of the CPP TAT-HuR-HNS3, which may be achieved at multiple levels. In the nucleus, the peptide competitively blocks HuR–PARP1 interaction, lowering the PARylation level of HuR, which attenuates the nuclear translocation of HuR. The mitigated cytoplasmic redistribution of HuR may also result from the perturbation of the recognition of HuR by export machinery by the

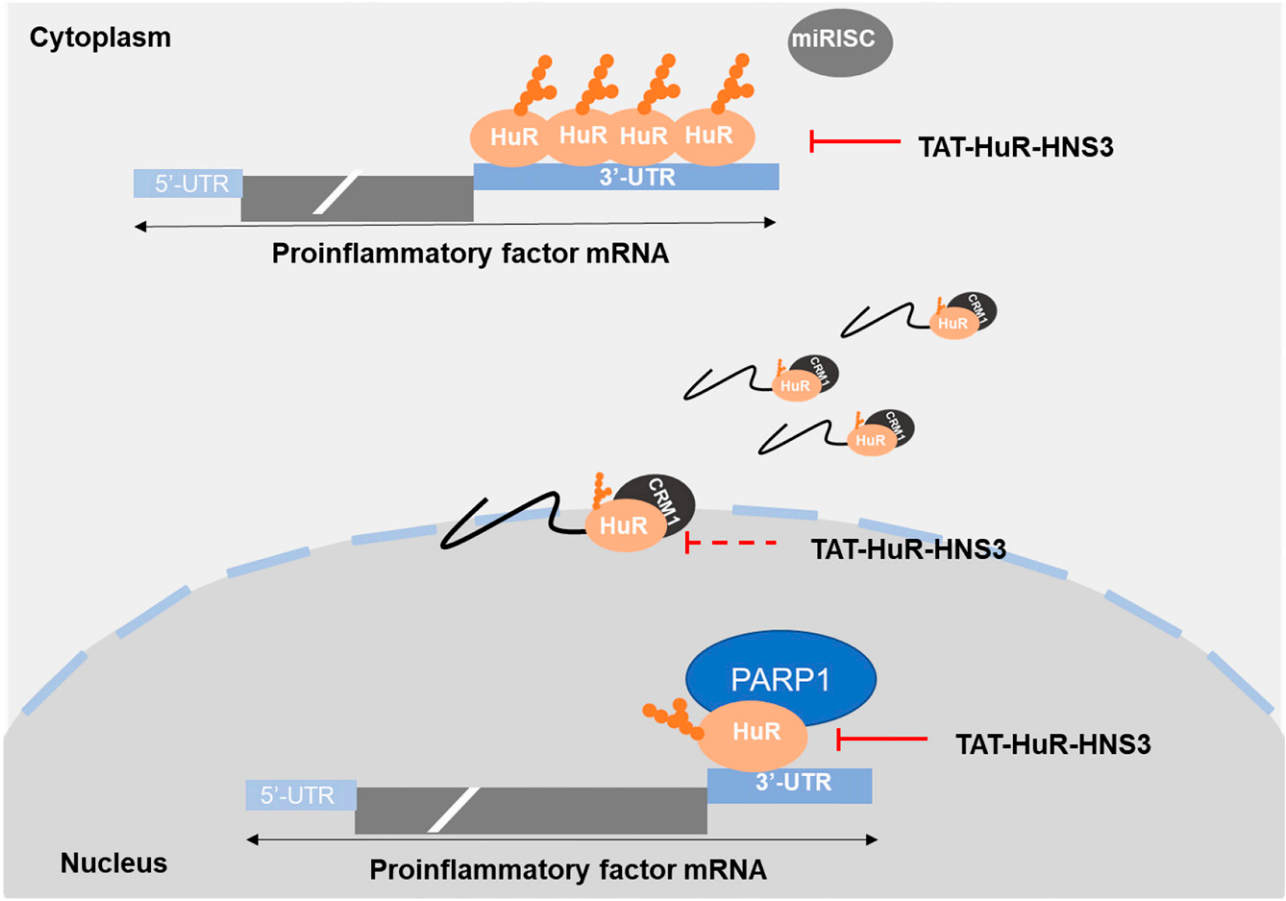

FIGURE 7. Schematic diagram showing roles of TAT-HuR-HNS3 in modulating inflammatory cytokine/chemokine expression. Modulation of proinflammatory gene expression by HuR can be achieved at multiple posttranscriptional levels, involving a range of HuR-interacting partners. The HNS domain of HuR is employed to mediate many of these interactions. TAT-HuR-HNS3, a C-terminal of HNS sequence–derived cell-penetrating peptide, may interrupt HuR interacting with PARP1 in the nucleus, impairing PARylation of HuR, and probably also blocks recognition of HuR by nuclear export machinery, collectively resulting in attenuated cytoplasmic shuttling of HuR. In the cytoplasm, TAT-HuR-HNS3 interferes HuR dimerization/oligomerization and facilitates the association of miRISC with RNAs, both of which promote RNA cleavage.

peptide. In the cytoplasm, TAT-HuR-HNS3 decreases HuR dimerization/oligomerization, allowing miRISC to outcompete HuR from the targets and to promote RNA decay (Fig. 7). In summary, given that higher abundance of the cytoplasmic HuR was seen in inflammation-related diseases or cancer (78,79), data of the current study suggest that HuR-HNS3 is a promising lead peptide for the development of specific anti-inflammatory agents used in anti-inflammation or anticancer therapies.

Acknowledgments

We thank Dr. Myriam Gorospe (Laboratory of Cellular and Molecular Biology, National Institute on Aging, National Institutes of Health) for providing GST and GST-HuR plasmids. We thank Dr. Lijuan Zhu (School of Foreign Language, Northeast Normal University) for critically editing this manuscript.

Disclosures

The authors have no financial conflicts of interest.

References

1. Änkö, M. L., and K. M. Neugebauer. 2012. RNA-protein interactions in vivo: global gets specific. *Trends Biochem. Sci.* 37: 255–262.
2. Gebauer, F., T. Schwarzl, J. Valcárcel, and M. W. Hentze. 2021. RNA-binding proteins in human genetic disease. *Nat. Rev. Genet.* 22: 185–198.
3. Barreau, C., L. Paillard, and H. B. Osborne. 2006. AU-rich elements and associated factors: are there unifying principles? *Nucleic Acids Res.* 33: 7138–7150.
4. Chen, C. Y., and A. B. Shyu. 1995. AU-rich elements: characterization and importance in mRNA degradation. *Trends Biochem. Sci.* 20: 465–470.
5. López de Silanes, I., M. Zhan, A. Lal, X. Yang, and M. Gorospe. 2004. Identification of a target RNA motif for RNA-binding protein HuR. *Proc. Natl. Acad. Sci. USA* 101: 2987–2992.
6. Blackinton, J. G., and J. D. Keene. 2016. Functional coordination and HuR-mediated regulation of mRNA stability during T cell activation. *Nucleic Acids Res.* 44: 426–436.
7. Brennan, C. M., and J. A. Steitz. 2001. HuR and mRNA stability. *Cell. Mol. Life Sci.* 58: 266–277.
8. Noh, J. H., K. M. Kim, K. Abdelmohsen, J. H. Yoon, A. C. Panda, R. Munk, J. Kim, J. Curtis, C. A. Moad, C. M. Wohler, et al. 2016. HuR and GRSF1 modulate the nuclear export and mitochondrial localization of the lncRNA RMRP. *Genes Dev.* 30: 1224–1239.
9. Srikantan, S., and M. Gorospe. 2012. HuR function in disease. *Front. Biosci.* 17: 189–205.
10. Herjan, T., P. Yao, W. Qian, X. Li, C. Liu, K. Bulek, D. Sun, W. P. Yang, J. Zhu, A. He, et al. 2013. HuR is required for IL-17-induced Act1-mediated CXCL1 and CXCL5 mRNA stabilization. *J. Immunol.* 191: 640–649.
11. Zhang, Z., A. Huang, A. Zhang, and C. Zhou. 2017. HuR promotes breast cancer cell proliferation and survival via binding to CDK3 mRNA. *Biomed. Pharmacother.* 91: 788–795.
12. Grammatikakis, I., K. Abdelmohsen, and M. Gorospe. 2017. Posttranslational control of HuR function. *Wiley Interdiscip. Rev. RNA* 8: e1372.
13. Chand, S. N., M. Zarei, M. J. Schiewer, A. R. Kamath, C. Romeo, S. Lal, J. A. Cozzitorto, A. Nevler, L. Scolaro, E. Londin, et al. 2017. Posttranscriptional regulation of *PARG* mRNA by HuR facilitates DNA repair and resistance to PARP inhibitors. *Cancer Res.* 77: 5011–5025.
14. Ouhara, K., S. Munenaga, M. Kajiya, K. Takeda, S. Matsuda, Y. Sato, Y. Hamamoto, T. Iwata, S. Yamasaki, K. Akutagawa, et al. 2018. The induced RNA-binding protein, HuR, targets 3′-UTR region of IL-6 mRNA and enhances its stabilization in periodontitis. *Clin. Exp. Immunol.* 192: 325–336.

15. Casolaro, V., X. Fang, B. Tancowny, J. Fan, F. Wu, S. Srikantan, S. Y. Asaki, U. De Fanis, S. K. Huang, M. Gorospe, et al. 2008. Posttranscriptional regulation of IL-13 in T cells: role of the RNA-binding protein HuR. *J. Allergy Clin. Immunol.* 121: 853–9.e4.
16. Ke, Y., Y. Han, X. Guo, J. Wen, K. Wang, X. Jiang, X. Tian, X. Ba, I. Boldogh, and X. Zeng. 2017. PARP1 promotes gene expression at the post-transcriptional level by modulating the RNA-binding protein HuR. [Published erratum appears in 2017 *Nat. Commun.* 8: 15191.] *Nat. Commun.* 8: 14632.
17. Song, X., X. Shi, W. Li, F. Zhang, and Z. Cai. 2020. The RNA-binding protein HuR in digestive system tumors. *BioMed Res. Int.* 2020: 9656051.
18. Young, L. E., A. E. Moore, L. Sokol, N. Meisner-Kober, and D. A. Dixon. 2012. The mRNA stability factor HuR inhibits microRNA-16 targeting of COX-2. *Mol. Cancer Res.* 10: 167–180.
19. Ishimaru, D., S. Ramalingam, T. K. Sengupta, S. Bandyopadhyay, S. Dellis, B. G. Tholanikunnel, D. J. Fernandes, and E. K. Spicer. 2009. Regulation of Bcl-2 expression by HuR in HL60 leukemia cells and A431 carcinoma cells. *Mol. Cancer Res.* 7: 1354–1366.
20. Chang, S. H., Y. C. Lu, X. Li, W. Y. Hsieh, Y. Xiong, M. Ghosh, T. Evans, O. Elemento, and T. Hla. 2013. Antagonistic function of the RNA-binding protein HuR and miR-200b in post-transcriptional regulation of vascular endothelial growth factor-A expression and angiogenesis. *J. Biol. Chem.* 288: 4908–4921.
21. Basu, A., D. Datta, D. Zurakowski, and S. Pal. 2010. Altered VEGF mRNA stability following treatments with immunosuppressive agents: implications for cancer development. *J. Biol. Chem.* 285: 25196–25202.
22. Xie, M., T. Yu, X. Jing, L. Ma, Y. Fan, F. Yang, P. Ma, H. Jiang, X. Wu, Y. Shu, and T. Xu. 2020. Exosomal circSHKBP1 promotes gastric cancer progression via regulating the miR-582-3p/HUR/VEGF axis and suppressing HSP90 degradation. *Mol. Cancer* 19: 112.
23. Platania, C. B. M., V. Pittalà, A. Pascale, N. Marchesi, C. D. Anfuso, G. Lupo, M. Cristaldi, M. Olivieri, F. Lazzara, L. Di Paola, et al. 2020. Novel indole derivatives targeting HuR-mRNA complex to counteract high glucose damage in retinal endothelial cells. *Biochem. Pharmacol.* 175: 113908.
24. Liu, R., K. Wu, Y. Li, R. Sun, and X. Li. 2020. Human antigen R: a potential therapeutic target for liver diseases. *Pharmacol. Res.* 155: 104684.
25. Zhou, H., S. Jarujaron, E. C. Gurley, L. Chen, H. Ding, E. Studer, W. M. Pandak, Jr., W. Hu, T. Zou, J. Y. Wang, and P. B. Hylemon. 2007. HIV protease inhibitors increase TNF-α and IL-6 expression in macrophages: involvement of the RNA-binding protein HuR. *Atherosclerosis* 195: e134–e143.
26. Dixon, D. A., N. D. Tolley, P. H. King, L. B. Nabors, T. M. McIntyre, G. A. Zimmerman, and S. M. Prescott. 2001. Altered expression of the mRNA stability factor HuR promotes cyclooxygenase-2 expression in colon cancer cells. *J. Clin. Invest.* 108: 1657–1665.
27. Nabors, L. B., G. Y. Gillespie, L. Harkins, and P. H. King. 2001. HuR, a RNA stability factor, is expressed in malignant brain tumors and binds to adenine- and uridine-rich elements within the 3′ untranslated regions of cytokine and angiogenic factor mRNAs. *Cancer Res.* 61: 2154–2161.
28. Durie, D., S. M. Lewis, U. Liwak, M. Kisilewicz, M. Gorospe, and M. Holcik. 2011. RNA-binding protein HuR mediates cytoprotection through stimulation of XIAP translation. *Oncogene* 30: 1460–1469.
29. Mazan-Mamczarz, K., S. Galbán, I. López de Silanes, J. L. Martindale, U. Atasoy, J. D. Keene, and M. Gorospe. 2003. RNA-binding protein HuR enhances p53 translation in response to ultraviolet light irradiation. *Proc. Natl. Acad. Sci. USA* 100: 8354–8359.
30. Fan, X. C., and J. A. Steitz. 1998. HNS, a nuclear-cytoplasmic shuttling sequence in HuR. *Proc. Natl. Acad. Sci. USA* 95: 15293–15298.
31. Toba, G., and K. White. 2008. The third RNA recognition motif of *Drosophila* ELAV protein has a role in multimerization. *Nucleic Acids Res.* 36: 1390–1399.
32. Ke, Y., X. Lv, X. Fu, J. Zhang, A. A. Bohio, X. Zeng, W. Hao, R. Wang, I. Boldogh, and X. Ba. 2021. Poly(ADP-ribosyl)ation enhances HuR oligomerization and contributes to pro-inflammatory gene mRNA stabilization. *Cell. Mol. Life Sci.* 78: 1817–1835.
33. Srikantan, S., K. Tominaga, and M. Gorospe. 2012. Functional interplay between RNA-binding protein HuR and microRNAs. *Curr. Protein Pept. Sci.* 13: 372–379.
34. Kim, J., K. Abdelmohsen, X. Yang, S. De, I. Grammatikakis, J. H. Noh, and M. Gorospe. 2016. lncRNA OIP5-AS1/cyrano sponges RNA-binding protein HuR. *Nucleic Acids Res.* 44: 2378–2392.
35. Tominaga, K., S. Srikantan, E. K. Lee, S. S. Subaran, J. L. Martindale, K. Abdelmohsen, and M. Gorospe. 2011. Competitive regulation of nucleolin expression by HuR and miR-494. *Mol. Cell. Biol.* 31: 4219–4231.
36. Simone, L. E., and J. D. Keene. 2013. Mechanisms coordinating ELAV/Hu mRNA regulons. *Curr. Opin. Genet. Dev.* 23: 35–43.
37. Kundu, P., M. R. Fabian, N. Sonenberg, S. N. Bhattacharyya, and W. Filipowicz. 2012. HuR protein attenuates miRNA-mediated repression by promoting miRISC dissociation from the target RNA. *Nucleic Acids Res.* 40: 5088–5100.
38. Zhuang, R., J. N. Rao, T. Zou, L. Liu, L. Xiao, S. Cao, N. Z. Hansraj, M. Gorospe, and J. Y. Wang. 2013. miR-195 competes with HuR to modulate *stim1* mRNA stability and regulate cell migration. *Nucleic Acids Res.* 41: 7905–7919.
39. Mukherjee, N., D. L. Corcoran, J. D. Nusbaum, D. W. Reid, S. Georgiev, M. Hafner, M. Ascano, Jr., T. Tuschl, U. Ohler, and J. D. Keene. 2011. Integrative regulatory mapping indicates that the RNA-binding protein HuR couples pre-mRNA processing and mRNA stability. *Mol. Cell* 43: 327–339.
40. Abdelmohsen, K., S. Srikantan, X. Yang, A. Lal, H. H. Kim, Y. Kuwano, S. Galban, K. G. Becker, D. Kamara, R. de Cabo, and M. Gorospe. 2009. Ubiquitin-mediated proteolysis of HuR by heat shock. *EMBO J.* 28: 1271–1282.
41. Anderson, P. 2010. Post-transcriptional regulons coordinate the initiation and resolution of inflammation. *Nat. Rev. Immunol.* 10: 24–35.
42. Kim, H. H., K. Abdelmohsen, A. Lal, R. Pullmann, Jr., X. Yang, S. Galban, S. Srikantan, J. L. Martindale, J. Blethrow, K. M. Shokat, and M. Gorospe. 2008. Nuclear HuR accumulation through phosphorylation by Cdk1. *Genes Dev.* 22: 1804–1815.
43. Yoon, J. H., K. Abdelmohsen, S. Srikantan, R. Guo, X. Yang, J. L. Martindale, and M. Gorospe. 2014. Tyrosine phosphorylation of HuR by JAK3 triggers dissociation and degradation of HuR target mRNAs. *Nucleic Acids Res.* 42: 1196–1208.
44. Li, H., S. Park, B. Kilburn, M. A. Jelinek, A. Henschen-Edman, D. W. Aswad, M. R. Stallcup, and I. A. Laird-Offringa. 2002. Lipopolysaccharide-induced methylation of HuR, an mRNA-stabilizing protein, by CARM1. *J. Biol. Chem.* 277: 44623–44630.
45. Lucchesi, C., M. S. Sheikh, and Y. Huang. 2016. Negative regulation of RNA-binding protein HuR by tumor-suppressor ECRG2. *Oncogene* 35: 2565–2573.
46. Hao, S., and D. Baltimore. 2009. The stability of mRNA influences the temporal order of the induction of genes encoding inflammatory molecules. *Nat. Immunol.* 10: 281–288.
47. Visnes, T., A. Cázares-Körner, W. Hao, O. Wallner, G. Masuyer, O. Loseva, O. Mortusewicz, E. Wiita, A. Sarno, A. Manoilov, et al. 2018. Small-molecule inhibitor of OGG1 suppresses proinflammatory gene expression and inflammation. *Science* 362: 834–839.
48. Jagtap, P., F. G. Soriano, L. Virág, L. Liaudet, J. Mabley, E. Szabó, G. Haskó, A. Marton, C. B. Lorigados, F. Gallyas, Jr., et al. 2002. Novel phenanthridinone inhibitors of poly(adenosine 5′-diphosphate-ribose) synthetase: potent cytoprotective and antishock agents. *Crit. Care Med.* 30: 1071–1082.
49. Rizzuti, M., M. Nizzardo, C. Zanetta, A. Ramirez, and S. Corti. 2015. Therapeutic applications of the cell-penetrating HIV-1 Tat peptide. *Drug Discov. Today* 20: 76–85.
50. Gump, J. M., and S. F. Dowdy. 2007. TAT transduction: the molecular mechanism and therapeutic prospects. *Trends Mol. Med.* 13: 443–448.
51. Wadia, J. S., and S. F. Dowdy. 2005. Transmembrane delivery of protein and peptide drugs by TAT-mediated transduction in the treatment of cancer. *Adv. Drug Deliv. Rev.* 57: 579–596.
52. Kanwar, J. R., J. Gibbons, A. K. Verma, and R. K. Kanwar. 2012. Cell-penetrating properties of the transactivator of transcription and polyarginine (R9) peptides, their conjugative effect on nanoparticles and the prospect of conjugation with arsenic trioxide. *Anticancer Drugs* 23: 471–482.
53. Gallouzi, I. E., C. M. Brennan, M. G. Stenberg, M. S. Swanson, A. Eversole, N. Maizels, and J. A. Steitz. 2000. HuR binding to cytoplasmic mRNA is perturbed by heat shock. [Published erratum appears in 2003 *Proc. Natl. Acad. Sci. USA* 100: 763.] *Proc. Natl. Acad. Sci. USA* 97: 3073–3078.
54. Evers, B., R. Drost, E. Schut, M. de Bruin, E. van der Burg, P. W. Derksen, H. Holstege, X. Liu, E. van Drunen, H. B. Beverloo, et al. 2008. Selective inhibition of BRCA2-deficient mammary tumor cell growth by AZD2281 and cisplatin. *Clin. Cancer Res.* 14: 3916–3925.
55. Fialcowitz-White, E. J., B. Y. Brewer, J. D. Ballin, C. D. Willis, E. A. Toth, and G. M. Wilson. 2007. Specific protein domains mediate cooperative assembly of HuR oligomers on AU-rich mRNA-destabilizing sequences. *J. Biol. Chem.* 282: 20948–20959.
56. Nawalpuri, B., S. Ravindran, and R. S. Muddashetty. 2020. The role of dynamic miRISC during neuronal development. *Front. Mol. Biosci.* 7: 8.
57. Deshmukh, P., S. Markande, V. Fandade, Y. Ramtirtha, M. S. Madhusudhan, and J. Joseph. 2021. The miRISC component AGO2 has multiple binding sites for Nup358 SUMO-interacting motif. *Biochem. Biophys. Res. Commun.* 556: 45–52.
58. Sibony, M., M. Abdullah, L. Greenfield, D. Raju, T. Wu, D. M. Rodrigues, E. Galindo-Mata, H. Mascarenhas, D. J. Philpott, M. S. Silverberg, and N. L. Jones. 2015. Microbial disruption of autophagy alters expression of the RISC component AGO2, a critical regulator of the miRNA silencing pathway. *Inflamm. Bowel Dis.* 21: 2778–2786.
59. Pantazopoulou, V. I., A. D. Delis, S. Georgiou, S. N. Pagakis, V. Filippa, E. Dragona, I. Kloukina, E. Chatzitheodoridis, J. Trebicka, A. D. Velentzas, et al. 2021. AGO2 localizes to cytokinetic protrusions in a p38-dependent manner and is needed for accurate cell division. *Commun. Biol.* 4: 726.
60. Schultz, C. W., R. Preet, T. Dhir, D. A. Dixon, and J. R. Brody. 2020. Understanding and targeting the disease-related RNA binding protein human antigen R (HuR). *Wiley Interdiscip. Rev. RNA* 11: e1581.
61. Pabis, M., G. M. Popowicz, R. Stehle, D. Fernández-Ramos, S. Asami, L. Warner, S. M. García-Mauriño, A. Schlundt, M. L. Martínez-Chantar, I. Díaz-Moreno, and M. Sattler. 2019. HuR biological function involves RRM3-mediated dimerization and RNA binding by all three RRMs. *Nucleic Acids Res.* 47: 1011–1029.
62. Yi, J., N. Chang, X. Liu, G. Guo, L. Xue, T. Tong, M. Gorospe, and W. Wang. 2010. Reduced nuclear export of HuR mRNA by HuR is linked to the loss of HuR in replicative senescence. *Nucleic Acids Res.* 38: 1547–1558.
63. Wang, J., A. B. Hjelmeland, L. B. Nabors, and P. H. King. 2019. Anti-cancer effects of the HuR inhibitor, MS-444, in malignant glioma cells. *Cancer Biol. Ther.* 20: 979–988.
64. Muralidharan, R., M. Mehta, R. Ahmed, S. Roy, L. Xu, J. Aubé, A. Chen, Y. D. Zhao, T. Herman, R. Ramesh, and A. Munshi. 2017. HuR-targeted small molecule inhibitor exhibits cytotoxicity towards human lung cancer cells. *Sci. Rep.* 7: 9694.
65. Skliris, A., O. Papadaki, P. Kafasla, I. Karakasiliotis, O. Hazapis, M. Reczko, S. Grammenoudi, J. Bauer, and D. L. Kontoyiannis. 2015. Neuroprotection requires the functions of the RNA-binding protein HuR. *Cell Death Differ.* 22: 703–718.
66. Habiba, U., T. Kitamura, A. Yanagawa-Matsuda, K. Hida, F. Higashino, Y. Ohiro, Y. Totsuka, and M. Shindoh. 2014. Cytoplasmic expression of HuR may be a valuable diagnostic tool for determining the potential for malignant transformation of oral verrucous borderline lesions. *Oncol. Rep.* 31: 1547–1554.
67. Bruzzoni-Giovanelli, H., V. Alezra, N. Wolff, C. Z. Dong, P. Tuffery, and A. Rebollo. 2018. Interfering peptides targeting protein-protein interactions: the next generation of drugs? *Drug Discov. Today* 23: 272–285.

68. Sorolla, A., E. Wang, E. Golden, C. Duffy, S. T. Henriques, A. D. Redfern, and P. Blancafort. 2020. Precision medicine by designer interference peptides: applications in oncology and molecular therapeutics. *Oncogene* 39: 1167–1184.
69. Yoshimaru, T., K. Aihara, M. Komatsu, Y. Matsushita, Y. Okazaki, S. Toyokuni, J. Honda, M. Sasa, Y. Miyoshi, A. Otaka, and T. Katagiri. 2017. Stapled BIG3 helical peptide ERAP potentiates anti-tumour activity for breast cancer therapeutics. *Sci. Rep.* 7: 1821.
70. Gallouzi, I. E., and J. A. Steitz. 2001. Delineation of mRNA export pathways by the use of cell-permeable peptides. [Published erratum appears in 2002 *Science* 296: 47.] *Science* 294: 1895–1901.
71. Xie, J., Y. Bi, H. Zhang, S. Dong, L. Teng, R. J. Lee, and Z. Yang. 2020. Cell-penetrating peptides in diagnosis and treatment of human diseases: from preclinical research to clinical application. *Front. Pharmacol.* 11: 697.
72. Frankel, A. D., and C. O. Pabo. 1988. Cellular uptake of the tat protein from human immunodeficiency virus. *Cell* 55: 1189–1193.
73. Ramsey, J. D., and N. H. Flynn. 2015. Cell-penetrating peptides transport therapeutics into cells. *Pharmacol. Ther.* 154: 78–86.
74. Gupta, B., T. S. Levchenko, and V. P. Torchilin. 2005. Intracellular delivery of large molecules and small particles by cell-penetrating proteins and peptides. *Adv. Drug Deliv. Rev.* 57: 637–651.
75. Mitchell, D. J., D. T. Kim, L. Steinman, C. G. Fathman, and J. B. Rothbard. 2000. Polyarginine enters cells more efficiently than other polycationic homopolymers. *J. Pept. Res.* 56: 318–325.
76. Kaplan, I. M., J. S. Wadia, and S. F. Dowdy. 2005. Cationic TAT peptide transduction domain enters cells by macropinocytosis. [Published errata appear in 2005 *J. Control Release* 107: 184–185 and 2005 *J. Control Release* 107: 571–572.] *J. Control. Release* 102: 247–253.
77. Bartlett II, R. L., S. Sharma, and A. Panitch. 2013. Cell-penetrating peptides released from thermosensitive nanoparticles suppress pro-inflammatory cytokine response by specifically targeting inflamed cartilage explants. *Nanomedicine (Lond.)* 9: 419–427.
78. Blaxall, B. C., L. D. Dwyer-Nield, A. K. Bauer, T. J. Bohlmeyer, A. M. Malkinson, and J. D. Port. 2000. Differential expression and localization of the mRNA binding proteins, AU-rich element mRNA binding protein (AUF1) and Hu antigen R (HuR), in neoplastic lung tissue. *Mol. Carcinog.* 28: 76–83.
79. Lang, M., D. Berry, K. Passecker, I. Mesteri, S. Bhuju, F. Ebner, V. Sedlyarov, R. Evstatiev, K. Dammann, A. Loy, et al. 2017. HuR small-molecule inhibitor elicits differential effects in adenomatosis polyposis and colorectal carcinogenesis. *Cancer Res.* 77: 2424–2438.